Norwegian University
of Life Sciences

Master's Thesis 2023 30 ECTS
Faculty of Science and Technology

Analysis of Natural Convection and High Voltage AC Cable Rating in Naturally Ventilated Tunnels

Anders Myklemyr
Environmental Physics and Renewable Energy

Preface

Presented here is the dissertation that culminates my Master's degree in Environmental Physics and Renewable Energy at the Norwegian University of Life Sciences (NMBU). The thesis was written during the spring of 2023 whilst data was collected from December of 2022 until February of 2023.

The work has been done in collaboration with the electrical power department at Sweco, who enabled the collection of data and provided expertise in the power cable field. The power cable site was provided by Lede, a distribution grid operator, who let me mount sensors at one of their naturally ventilated power cable tunnel locations.

I would like to direct a special thanks to my supervisor Jorge M. Marchetti at NMBU for invaluable input and interesting discussions during the writing process. I would also like to thank Anders Ballari at Sweco for providing the idea for the master thesis as well giving me vital support during the entire dissertation proceeding. Anders has also contributed with power cable expertise, vital for this thesis. Deep gratitude also goes to Ørjan Bø, who has been our contact at Lede. He helped us install the sensors as well as providing valuable data about the cable and the site of its installment.

Lastly I would like to express my deepest and sincere gratitude to my wife who has given me unquestionable support during the writing process as well as during the course of the entire Master's degree. I thank you for your sacrifice and for always believing in me.

Thank you!

I sincerely hope you will enjoy reading.

NMBU, Ås 17th of April

Anders Myklemyr

Abstract

High voltage (HV) underground power cables are an important part of the power grid. In recent years, the necessity of optimization of power flow within the grid has increased significantly. The transition to renewable energy as well as the growth of electricity demand has resulted in high loads on the existing grid network. In order to optimize the ampacity of underground power cables, a good understanding of their thermal environment is needed. However, the occurrence and effect of wind flow in naturally ventilated cable tunnels has not been researched extensively. To further explore this phenomenon, two temperature sensors and a wind sensor were installed at an HVAC power cable tunnel site. The power cable site contains a three phase 2000 mm^2 aluminum cable, rated for 132 kV, with cross-linked polyethylene (XLPE) insulation.

The collection of temperature and wind data were compared to theoretical models to investigate whether the models could be used for future estimation of wind speed in cable tunnels. A validation of the IEC 60287-2-3[1] [1] model, for calculating the ampacity rating, was also explored. The wind sensor registered a maximum wind speed of 0.7 $\mathrm{m\,s}^{-1}$ at the tunnel exit, which coincided with the theoretical calculations, for naturally induced wind. The calculations were made using an equivalent diameter as the tunnel diameter. However, more data is needed to verify the model.

The cable at the sensor site had a steady but low load. The load current was around 300 A, compared to the maximum permissible load of 985 A. A cable with a higher load current would have resulted in higher cable temperatures, leading to clearer wind data. The IEC model, used for ampacity and temperature calculations, correlated with the collected temperature data with an error of ca 20 %, meaning that the IEC model is in good agreement with the collected data at this specific site. Thus the IEC model can be used to establish an ampacity rating for an HVAC cable laid in an underground tunnel. Furthermore, the calculation of naturally induced wind flow can be used as an indication of wind speed in cable tunnels, until further verified.

[1]IEC 60287-2-3 ed.1.0 “Copyright © 2017 IEC Geneva, Switzerland. www.iec.ch”

Sammendrag

Høyspente jordkabler er viktige elementer i kraftnettet og nødvendigheten for å optimere kraftflødet gjennom kraftnettet har økt signifikant de seneste årene. Overgangen til fornybar energi og den økte etterspørselen etter mer elektrisitet har resultert i høy belastning av det eksisterende kraftnettet. For å avlaste nettet, kreves optimering av kraftflødet. Høyspente jordkabler er en måte å overføre strøm på og for å optimere flyten gjennom disse trengs en forståelse for omgivelsene som kabelen ligger i. Dog, har det ikke blitt foretatt omfattende forskning på forekomsten og effekten av vindhastighet gjennom naturlig ventilerte kabelkulverter. For å undersøke dette feltet nermere, har to temperatursensorer og en vindsensor blitt installert ved en HVAC kabel i en naturlig ventilert tunnel. Kablene består av tre faser á 132 kV med 2000 mm^2 aluminiums ledere innkapslet i XLPE isolering.

Innsamling av temperatur og vind data ble sammenlignet med teoretiske modeller. Vindhastigheten i tunnelen ble predikert og sammenlignet med dataene. Det ble også foretatt en vurdering av treffsikkerheten for IEC 60287-2-3[1] [1] modellen, for estimering av strømkapasiteten i kabelen. Vindsensoren registrerte en maksimal vindhastighet på 0.7 $m\,s^{-1}$ ved utløpet av tunnelen. Dette stemte med den teoretiske kalkulerte verdien for vind gjennom naturlig ventilerte kulverter, ved bruk av en ekvivalent diameter som diameter på tunnelen. Dog, kreves det mer vind data for å verifisere modellen.

Kabelen ved sensorlokasjonen hadde en jevn men lav last. Lasten på kabelen var omtrent 300 A, sammenlignet med maksimal tilatte last som var 985 A. En kabel med høyere strømmer ville ha resultert i høyere kabeltemperaturer som videre hadde gitt mer vinddata. IEC modellen, som brukes for estimering av strømkapasiteten i kabelen korrelerte med den innsamlede dataen med en kalkulert feilmargin på ca 20 %. Dette betyr at IEC modellen stemmer godt med dataene for denne spesifikke kabellokasjonen. Dette gir at IEC modellen er en god metode for å fastslå strømkapasiteten til en underjordisk kabel forlagt i ventilert tunnel. Videre gir beregningen for den teoretisk induserte vindhastigheten en indikasjon på vad som kan forventes, frem til modellen har blitt verifisert med mer data.

Nomenclature

AC	Alternating Current
DTS	Distributed Temperature Sensing
ECC	Earth Continuity Conductor
FEM	Finite Element Method
GHG	Greenhouse Gases
HV	High Voltage
HVAC	High Voltage Alternating Current
IEA	International Energy Agency
IEC	International Electrotechnical Commission
MAPE	Mean Absolute Percentage Error
MRS	Minimum Required Strength
OTDR	Optical Time Domain Reflectometry
PD	Partial Discharge
PE	Polyethylene
SDR	Standard Dimension Ratio
XLPE	Cross-Linked Polyethylene

Contents

List of Figures

List of Tables

1 Introduction

The world is facing several dire challenges that could define the future development of our planet. At present, humans have caused a global warming of approximately 1 °C above pre-industrial levels. The warming of the planet is likely to continue to 1.5 °C and above [2, 3]. To prevent the continued warming of the planet, the majority of the world has agreed to cut emissions in an attempt to stop global warming. At the same time, the world population is growing and so is the energy demand. The problem the world is facing is two-sided. Emissions have to be cut while simultaneously increasing energy production worldwide. If our generation fails at this task, severe consequences will follow. A warmer climate will lead to reduced access to food and water, higher ocean levels and more extreme weather [4]. Changing our very foundation for life on earth.

In order to achieve the goals of the Paris-Agreement [5], greenhouse gas emission (GHG) emissions have to be drastically reduced and fossil fuels need to be phased out [5]. As of 2018, fossil fuels accounted for 75 % of global GHG emissions [4]. Energy generation as well as energy used in industrial processes and for transportation need to transition from burning fossil fuels to using renewable energy. Electricity is an energy carrier and when generated from renewable sources it is considered a vital part of the fossil free future [4]. To achieve net zero emissions, a report from the International Energy Agency (IEA), states that 90 % of electricity generation in 2050 need to stem from renewable sources [6]. IEA also claims that global electricity demand will increase by 80 % between 2020 and 2050. To support this exploding demand for electricity, investments in the electricity grids are set to triple by 2030 and continue to be at elevated levels until the net zero scenario in 2050 [6].

The electric grid is an entity that transfers electricity through either overhead lines or underground power cables [7]. This thesis will focus on underground power cables. The grid needs to adapt to the fast pace of electrification which is why it is more important than ever to utilize the current infrastructure's capacity to its fullest. For HVAC cables in tunnels underground, it means having a detailed model for the current carrying capacity calculations [8].

The permissible current rating is largely dependent on the thermal properties of the medium surrounding the power cables. Some underground power cables need to traverse regions of less favourable thermal properties. As a result, cable temperatures can increase to a point where they surpass the design thermal limit [9]. For example, an asphalt-covered parking lot crossing may result in an increase of the conductor temperature by up to 10 °C, given similar soil conditions as outside the crossing. Consequently, the ampacity rating of such a conductor may be reduced by up to 40 % [10]. For a cable route, the current permissible rating is based on the section of the route where the least favourable

thermal conditions are present. Street crossings or deep tunnels are examples of regions where the cable can be thermally limited. One solution, to reduce the thermal limitations, is to fill the cable tunnel with thermal backfill to improve the thermal properties of the medium surrounding the cables [9]. Another solution is to let air cool the cable.

To cool the cable using air, the HV cable can be placed in naturally ventilated tunnels. The naturally ventilated tunnels can be used for road crossings, for traversing uneven terrain or as a bored hole through a mountain. In these tunnels the cables are surrounded by air which flows naturally through the tunnel via an inlet and outlet. A cut out view example of a bore hole tunnel through a mountain is depicted in Figure 1.1.

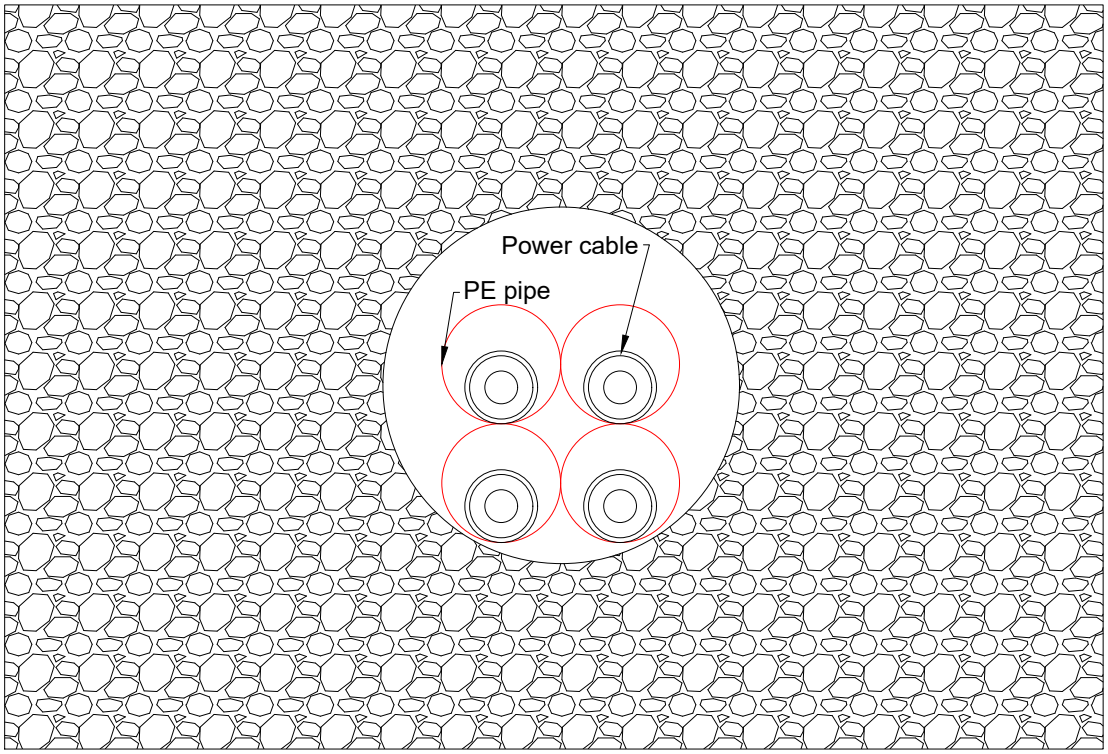

Figure 1.1: Example cut out view of a bore hole with plastic pipes containing power cables of three phases and one reserve phase. The bore hole is surrounded by mountain.

A challenge for naturally ventilated tunnels is that standstill air has different thermodynamic properties from rock or other thermal backfill. The thermal conductivity of rock is normally in the range of $0.4\,\mathrm{Wm^{-1}K^{-1}}$ to $7.00\,\mathrm{Wm^{-1}K^{-1}}$. The lower values are true for gravel and sand while the higher numbers are reserved for rock with a high quartz content. In comparison, still air has a thermal conductivity of around $0.026\,\mathrm{Wm^{-1}K^{-1}}$ [11]. The higher thermal conductivity of the rock means that a cable surrounded by rock will be cooled more effectively than a cable surrounded by still air. At present, most calculations of air filled cable tunnels are made with standstill air to simplify the process.

This can make cable tunnels with air a common thermal bottleneck when performing ampacity calculations along a HV-cable route. However, with a natural flow of air the convective heat transfer coefficient h_c of the air increases significantly as shown in Figure 1.2, calculated by using equation 1 [12]. In the equation, V is the wind speed in [m/s]. The increased heat transfer can aid in improving the ampacity of a power cable.

$$h_c = 12.12 - 1.16V + 11.6\sqrt{V} \qquad [\mathrm{W\,m^{-2}\,K}] \quad (1)$$

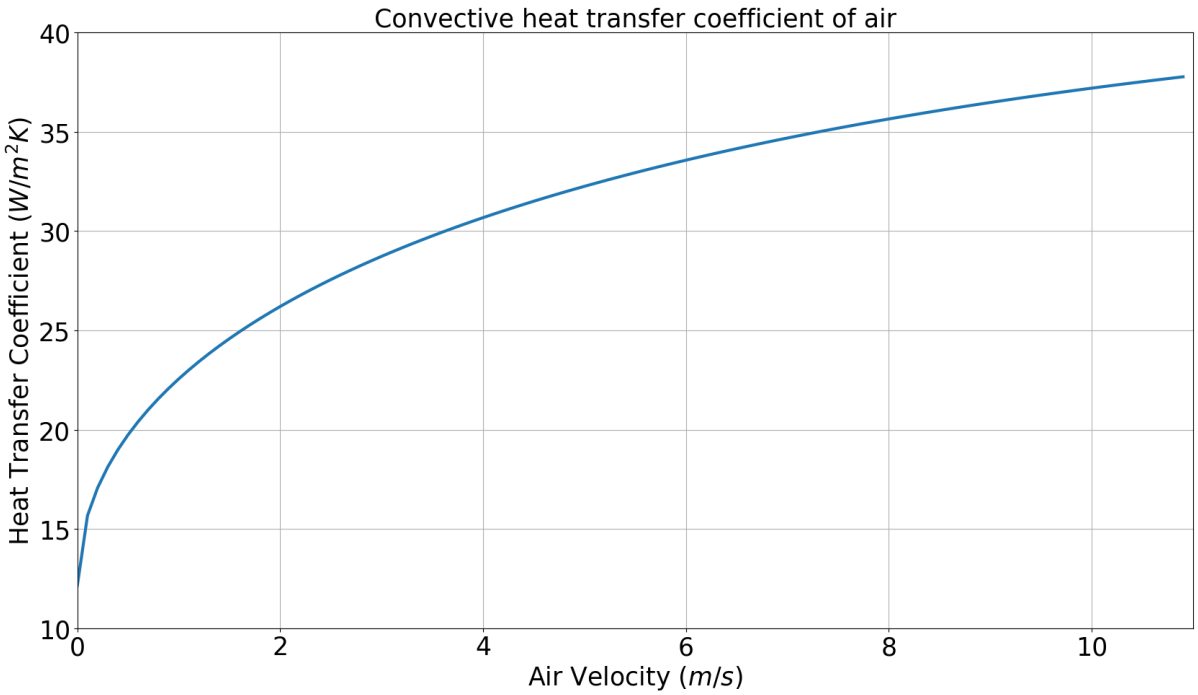

Figure 1.2: Approximation of the heat transfer coefficient as air velocity changes. Calculated using equation 1.

Ampacity calculations in naturally ventilated tunnels are normally made with the IEC 60287-1-1[2] method for standstill air, published by the International Electrotechnical Commission (IEC), using steady state [13, 14]. This method does not take into account the effects that naturally moving air may have on the ampacity of the cable. For naturally ventilated tunnels the lesser used IEC 60287-2-3[1] can be utilized, but few studies have been made on the applicability of these calculations on existing cable tunnels. The amount of natural ventilation occurring in such a tunnel is also generally unknown. This makes naturally ventilated HV cable tunnels an interesting area of research. By gaining a deeper understanding of the natural ventilation through a cable tunnel, the HV cables might be utilized closer to their full capacity.

[2]IEC 60287-1-1 ed.2.0 "Copyright © 2006 IEC Geneva, Switzerland. www.iec.ch"

1.1 Scope of Thesis

This thesis aims to improve the knowledge of natural movement of air in a cable tunnel caused by thermal differences due to the heat from a power cable. The aim is also to explore the cooling effect that naturally convective air has on the cable in terms of ampacity rating. Furthermore, the amount of induced air flow that a power cable can generate will be investigated.

Collection of data has been done for a power cable laid in a tunnel bored through a mountain. The tunnel has ventilation goose necks located at the start and end points of the tunnel. Sensors have been fitted which measure the inlet and outlet temperatures as well as the outlet wind speed of the tunnel. There is also a DTS-fiber laid beside the cable that measures the temperature of the cable for every meter in axial direction. Data of the current flowing through the cable will also be obtained. These measuring points are used for comparison with the IEC 60287-2-3[1] method for calculating the continuous current rating for cables of different voltages installed in ventilated tunnels. The tunnel site is further described in the methodology section.

2 Theory

The electric grid is a transmission system for electrical power that can be sorted into three major categories: substations with transformers and connections between the substations consisting of overhead transmission lines and underground power cables. This thesis will focus on underground power cables. The underground power cables are normally used in urban areas or where overhead transmission lines are not suitable [15]. The theory section of this thesis will delve into the construction of high voltage power cables and heat transfer mechanisms of the IEC 60287-2-3[1] method [1]. The method for calculation of ampacity rating in naturally ventilated tunnels will also be presented in section 2.4. Section 2.5 will present the live power cable investigated in this thesis.

2.1 High Voltage Cable Construction

A HV power cable is mainly composed of a conductor, a dielectric or insulation and a sheath [16]. A drawing of the primary components of a power cable is shown in Figure 2.1.

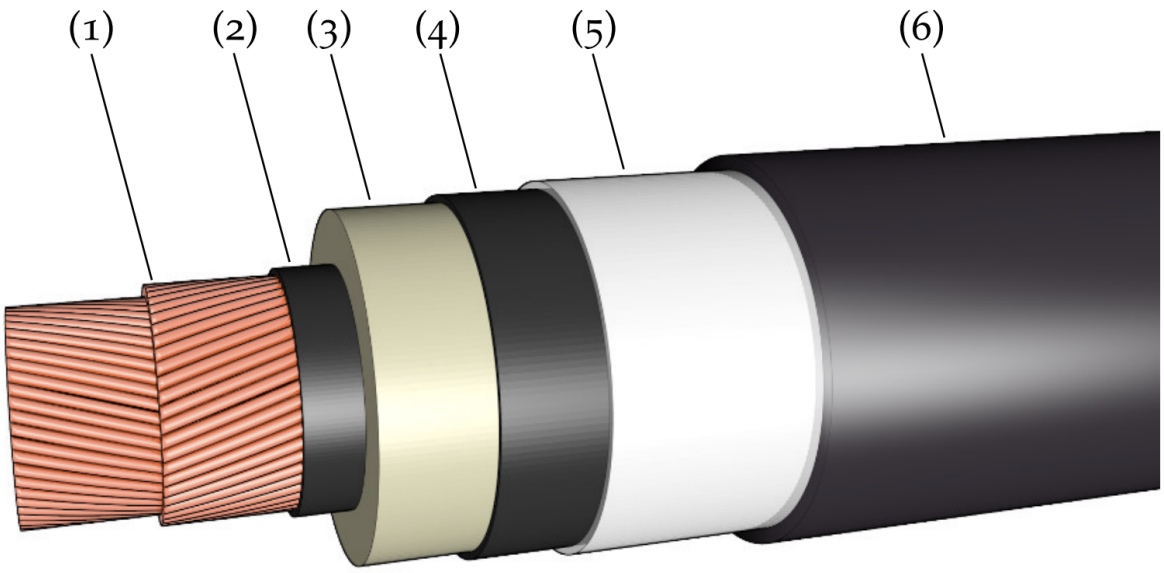

Figure 2.1: Drawing of the main components of a power cable. (1) Conductor, (2) conductor sheath, (3) insulation, (4) insulation sheath, (5) metallic sheath, (6) outer polymeric sheath [17].

The conductor (1) at the centre of the cable is what carries the electrical current and it is usually constructed of copper or aluminium, which are high conductivity materials. The conductor needs to be designed to enable bending of the cable and to minimize losses. The conductor sheath (2) and insulation sheath (4) are typically made of graphite, a semi-conductive material. The sheaths ensure an even radial electric field dispersal over the insulation material. The two most common types of insulation (3) are impregnated paper and extruded polymer [17]. The metallic sheath (5) is mainly a layer that prevents

moisture from entering the insulation. It also allows for earth return currents to flow [18]. Lastly the purpose of the outer polymeric sheath (6) is mechanical protection and moisture ingress prevention [17]. The conductor, insulation and semi-conductive sheaths will be further delved into in the following sections.

2.1.1 Conductor

The most common materials in a conductor are aluminium and copper. They possess high conductivity and are readily available in the earth's crust. Copper has the highest conductivity of the two but aluminium has become the most used conductor material due to its lesser weight, lower cost and high availability. The lower conductivity of aluminium means that for the same ampacity rating, a conductor with a larger cross section has to be selected in comparison to copper. Even though more material is used in an aluminium conductor, it is still more competitive considering both price and weight of the power cable [15].

The metal of choice is processed into strands which are subsequently put together to form a larger conductor. A common design of the conductor is called a Milliken type conductor. Figure 2.2 shows a cross section of a Milliken conductor. It was first suggested by Humphreys Milliken in 1933 [17].

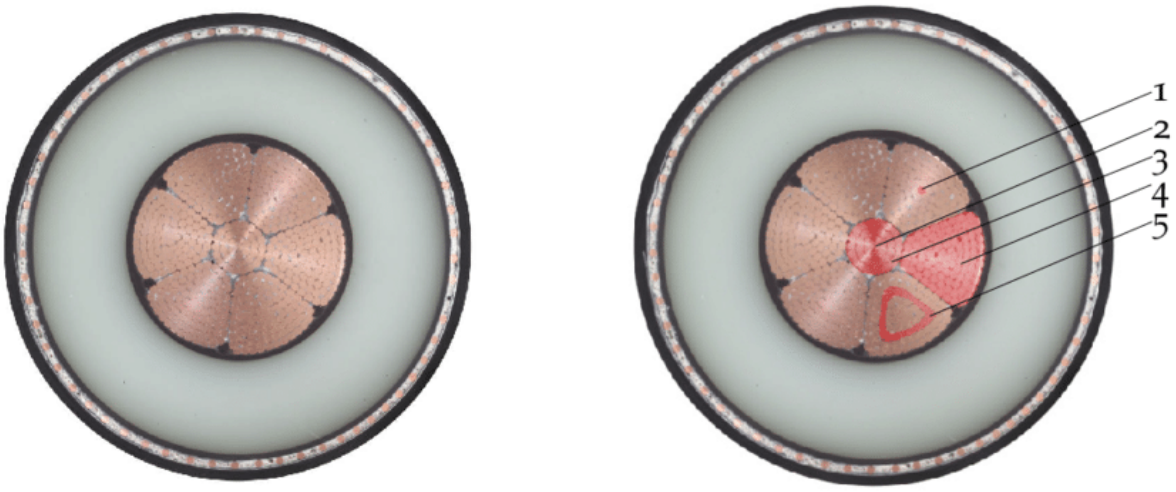

Figure 2.2: The figure shows a Milliken type conductor. The right portion highlights the details where the numbers represent: 1) single strand, 2) core of the cable, 3) one strand in the core, 4) segment of the whole conductor, 5) layer in a segment [17].

The purpose of the design is to reduce AC losses, typically for conductors with cross sections larger than 1000 mm^2. The Milliken design allows the strands to be transposed such that the total induction of each strand is similar. Transposing multiple strands means that every strand takes each position of the cross section for the same distance along the cable. This enables the current to be distributed equally between the strands. Each strand is insulated from one another by an oxidation layer to prevent currents from

flowing between strands. To achieve the transposition, the conductor is split into pie shaped segments, insulated from each other. The pie segments are then twisted around their own centre and are simultaneously twisted around the center core of the cable [17].

For larger cross sections, the current density in the center of the conductor is near zero. This is due to the fact that the center conductor strands never reach the periphery of the cable and thus, due to the skin effect of AC current, little current flows in the center. The skin effect is a physical phenomenon where the current density tends to peak closer to the surface of the conductor and hence decrease radially towards the centre. The skin effect as a function of frequency is visualized in Figure 2.3, showing that the skin effect is most prominent for AC currents with higher frequency [17]. Since little current flows in the center conductor it is possible to remove it in order to reduce losses [17]. This is done in some overhead lines where tensile strength is valued. In these cases the conducting core can be replaced with steel that has a high longitudinal strength which minimizes sag on power lines [19]. The Norwegian grid operates at a frequency of 50 Hz [20]. In contrary to a hollow construction, a Milliken construction can be used which minimizes the skin effect by equally splitting the current amongst each segment [15].

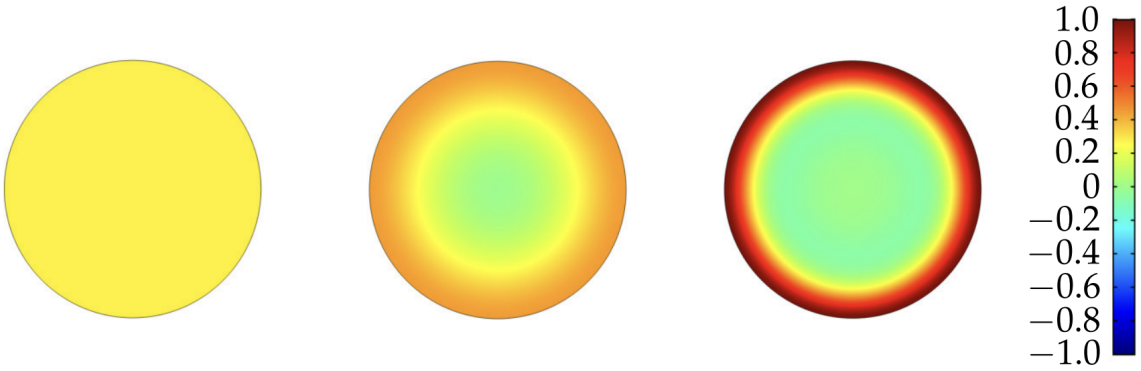

Figure 2.3: Visualization of the skin effect in relation to frequency. The color indicates different levels of current density. The left figure has a frequency of 0 Hz. The Middle has a frequency of 50 Hz and the right picture is at 300 Hz [17].

2.1.2 Semi-Conductive Sheaths

As observed in Figure 2.1, the conductor sheath surrounds the inner conductor and the insulation sheath covers the dielectric. The function of the conductor sheath is to give the conductor a smooth contour without imperfection. A conductor surface without screen results in a wavy surface which increases electrical stress and can cause failure of the cable over time. To create this semi-conductive screen, high-quality carbon is used. It is then mixed with a base polymer to make it conductive and to achieve a smooth surface [15]. The insulation sheath together with the conductor sheath enables a homogeneous electric field distribution in the insulation [17].

2.1.3 Insulation

The insulating material need to fulfill a few properties. It needs to endure high AC impulse voltages and to perform for a long time. The power loss in the insulating material should be kept to a minimum. The material of choice also needs to have resistance to treeing and corona [15]. Additionally, the power cable needs to be flexible and to resist mechanical abrasion and to tackle diverse environmental conditions, hence the insulation material has to be designed to meet these criteria [15].

Corona is the ionization occurring in a gas which surrounds a conductor or insulation surface with a high electric potential. This ionization is regularly audible in the presence of HV power lines [21]. It occurs when a gas is put under heavy electric field stress but not enough for the electric field to bridge the dielectric [21]. This means that no electric arc will form, instead the corona phenomenon appears as a blue glow.

Treeing is a phenomenon that occurs in insulation materials and is the main cause of failures in HV power cables. Treeing in XLPE insulation is shown in Figure 2.4. Treeing stems from gas voids or mechanical defects. In these tiny regions the electric field can be distorted causing small partial discharges which can lead to the occurrence of a tree-like destruction of the insulation material [22]. Partial discharge is an electrical breakdown, that does not fully traverse the dielectric gap between two electrodes, of a gas filled void inside a solid insulation material. PD occurs due to an electric field strength that surpasses the dielectric strength of that region. The gas filled voids have a lower dielectric constant than the insulation material itself. The voids also contain edges and corners which increases the stress of the electric field thus increasing the risk of PD. Electromagnetic radiation and high-speed electrons are what can cause damage to the insulation when a PD occurs. The PD causes deterioration of the walls of the gaseous voids and as more PDs occur, channels form that eventually takes the form of trees. Nearly all insulation materials contain voids and impurities where PDs can occur. It is nearly impossible to prevent PDs altogether, however the occurrence of PDs can be limited to a level that does not affect the overall lifetime of the insulation and the cable. To limit the occurrence of PDs, emphasis is laid on material selection and processing of the insulation. This allows a minimization of the number and size of the voids [21].

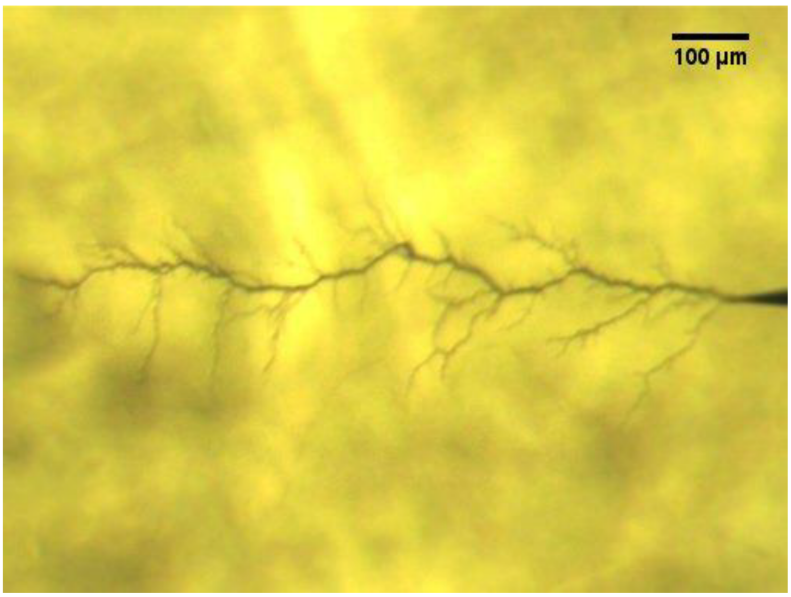

Figure 2.4: Visualization of the treeing phenomenon in XLPE insulation. [23]

The most common insulation material for HVAC cables is polymers and especially XLPE. It was invented in 1963 and it was proven that cross-linking of polyethylene molecules improved the material properties greatly, in comparison to regular PE. The new XLPE allowed for a higher operating temperature, up to 90 °C to 95 °C [15]. The XLPE insulation can also withstand short-circuit temperatures of up to 250 °C, making these cables able to safely transmit high currents [24]. Compared to regular PE, AC breakdown voltage was improved and the AC voltage impulse levels elevated. These improvements are valid as long as the XLPE is contamination free, hence reducing contamination is a vital part of the manufacturing process [15]. XLPE insulated HV cables are rated to have a life span of 40 years [25].

2.2 DTS-Fiber Temperature Sensor

A method to survey the cable's environment and to monitor its health is by usage of an optical fiber and the distributed temperature sensing method (DTS). Underground cables are subjected to various loads, ever changing thermal conditions as well as mechanical effects during its lifetime. The vulnerable part of the cable is the insulation which might suffer degradation due to the previous stated effects of treeing. In worst case, the degradation ultimately leads to breakdown of the insulation. It is therefore of great significance to monitor the temperature of the cable closely. This can be achieved using a DTS method, which produces a temperature profile along the cable. The most common technique, within DTS, is the optical time domain reflectometry method (OTDR) [24]. A schematic view of a DTS sensor is presented in Figure 2.5. A DTS system uses a detector that receives data from multiple and separate measurement points along the cable. The fiber

cable acts as a sensor in itself. The method is based on light travelling through the fiber, hence the technique is immune to electromagnetic interference. The fiber is also resistant to corrosion which is of importance when measuring the temperature of an underground power cable in a moist environment [24]. The DTS method uses pulses of light with a certain frequency which radiates through the fiber. Different scattering phenomena occur. One of them is Raman scattering. It occurs due to molecular and volumetric vibrations which makes Raman scattering closely related to temperature. The detector measures the frequency difference of incident and scattered photons. The frequency shift is correspondent to the vibration frequency of the molecules in the fiber. This is what ultimately gives the temperature profile along the cable. Raman scattering can form at different positions in the fiber and the scattering radiates evenly in all directions. Positioning of a scattering occurrence can be done using the the time difference between the sent and incident light pulse [26].

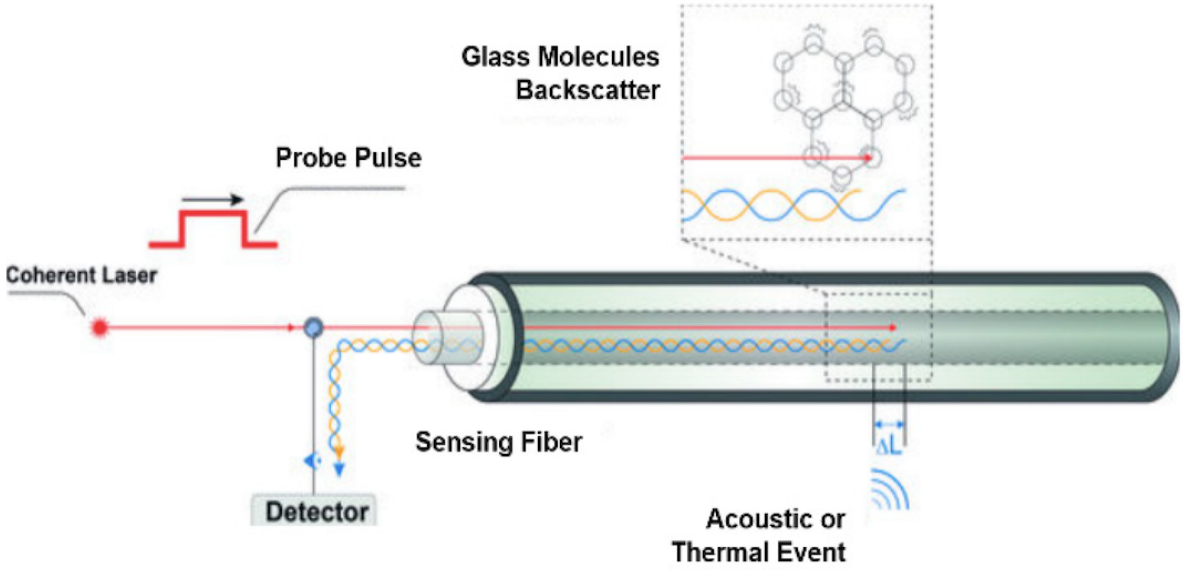

Figure 2.5: Representational view of a DTS-fiber system. [27]

2.3 Induced Tunnel Wind

For naturally ventilated tunnels, the wind may play a major role in improving the thermal environment of the power cable. The wind induced by the heat generated by a cable in an underground tunnel can be approximated by the equations in this section. At the ends of the power cable tunnel, vertical pipes can be fitted containing air columns of different temperatures. The temperature difference is due to the heat generated by the cable, hence the air columns have different densities. The density differences causes different gravitational forces, acting on the air column, which in turn leads to air movement. The density variation that leads to air movement is described mathematically in the following equations. This system finally leads to a steady state condition where a constant wind

velocity is established, caused by the air temperature increase along the cable length. A schematic view of a cable tunnel where natural air flow occurs is shown in Figure 2.6. The figure is linked to the subsequent equations in this subsection.

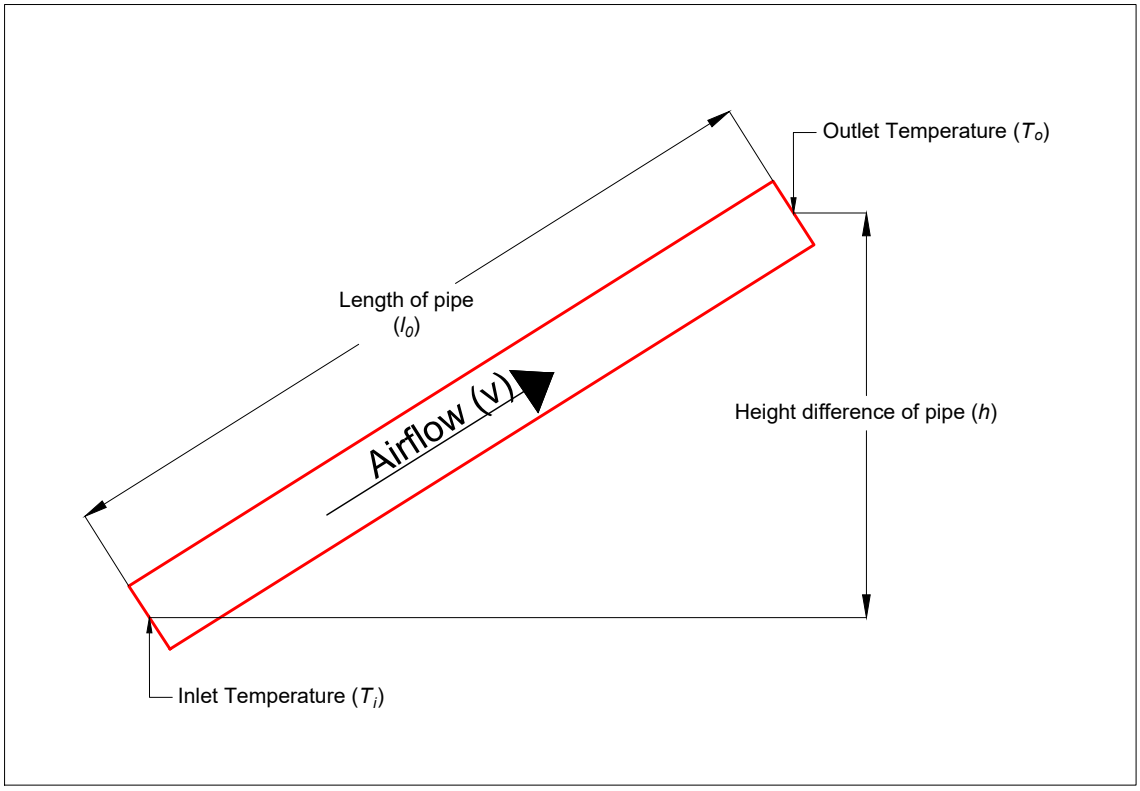

Figure 2.6: Figurative representation of naturally induced wind in a power cable tunnel, presenting variables included in equations 2, 3 and 6.

The pressure difference, as a result of the difference in air densities of the two air columns, can be modeled using

$$\begin{aligned} \Delta P &= g \cdot \Delta h \cdot [\rho(\theta_{in}) - \rho(\theta_{out})] \\ &= \Delta h \cdot \left(\frac{1}{T_{in}} - \frac{1}{T_{out}}\right) \cdot 3417.12, \end{aligned} \qquad [\mathrm{Pa\,K\,m^{-1}}] \quad (2)$$

where g is the gravitational constant, Δh is the height difference in [m] of the inlet and outlet ventilation pipes and T_{in} and T_{out} are the air temperatures in [°C] at the inlet and outlet in [K]. Furthermore, $\rho(\theta_{in})$ and $\rho(\theta_{out})$ are the densities of air, in $[\mathrm{kg\,m^{-3}}]$, at the inlet and outlet respectively as a function of the inlet and outlet temperatures [28]. The pressure difference causes air to circulate and the velocity of that air can be estimated by

$$V = \sqrt{\frac{2 \cdot \Delta P \cdot D_{eq}}{L \cdot \rho(\bar{\theta}) \cdot f_c}}, \qquad [\mathrm{m\,s^{-1}}] \quad (3)$$

where D_{eq} is an equivalent diameter, in [m], calculated using the difference in area between the cable pipe and the conductors obstructing the air flow in the pipe. The equivalent diameter is used as an approximation that models a diameter of a cable pipe without obstructions. The equivalent diameter is used to estimate the induced wind velocity in the pipe. Furthermore, $\rho(\theta)$ is the density of air as a function of temperature. $\rho(\bar{\theta})$ is a median value over the length of the cable and f_c is a friction coefficient of the air flow. Finally, L is the total pipe length in [m] [9]. The density of air inside the tunnel can be approximated by

$$\rho(\bar{\theta}) = \frac{352.64}{\bar{\theta} + 273}, \qquad [\mathrm{kg\,m^{-3}}] \quad (4)$$

where the average temperature along the cable ($\bar{\theta}$) is given in [°C] [9].

The friction coefficient is given by

$$f_c = \alpha \cdot [1.82 \cdot log(Re) - 1.64]^{-2}, \quad (5)$$

where Re is Reynolds number given in equation 12 [9]. Reynolds number gives an indication on whether the flow of a fluid is laminar or turbulent [29]. α is a constant and is set to 1 for nonmetallic pipes [10]. Lastly the total pipe length of the system is given by

$$L = l_0 + 2 \cdot \Delta h, \qquad [\mathrm{m}] \quad (6)$$

where l_0 is the length of the cable tunnel in [m] [9].

2.4 IEC 60287 Calculation of Ampacity in Ventilated Tunnels

This section will cover the method composed by the IEC for calculating the ampacity of a power cable in a ventilated tunnel using IEC 60287-2-3[1] [1], IEC 60287-2-1[3] [30] and IEC 60287-1-1[2] [13]. Where IEC 60287-2-3[1] covers the method for calculating ampacity in ventilated tunnels and IEC 60287-2-1[3] delves into calculations of thermal resistances of the cable. Lastly IEC 60287-1-1[2] presents a general method for calculating current rating of cables buried directly in the ground, in ducts, troughs or in steel pipes where natural or forced ventilation does not occur. For current rating in ventilated tunnels, only steady state is considered in this dissertation. Steady state refers to the case where the inlet air temperature and the cable loads are constant for a sufficient period for steady temperatures to be reached [1]. All equations in the following sections are reproduced with permission from the IEC.

[3]IEC 60287-2-1 ed.2.0 "Copyright © 2015 IEC Geneva, Switzerland. www.iec.ch"

2.4.1 Heat Transfer

The modes of heat transfer covered in the IEC 60287-2-3[1] method are presented in Figure 2.7 and they include radial heat transfer by conduction within the cable (1), heat transfer by radiation from the cable surface to the tunnel wall (2) and heat transfer by convection from the cable surface to the air inside the tunnel (3). Finally, the method includes heat transfer by convection from the air inside the tunnel to the tunnel wall (4) as well as longitudinal heat transfer by convection as a result from either forced or natural flow of air along the tunnel [1].

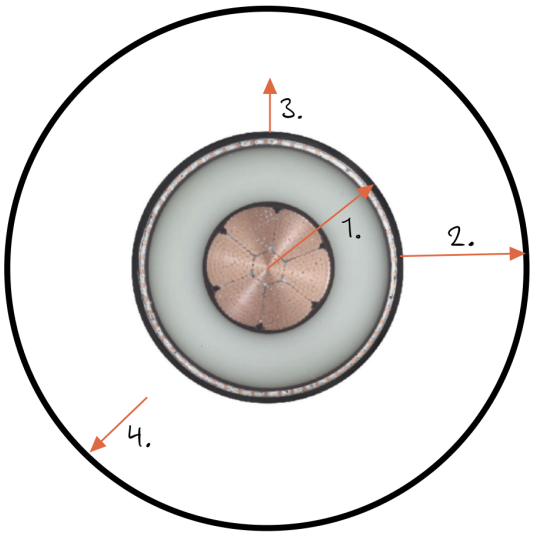

Figure 2.7: Modes of heat transfer included in the IEC60287-2-3[1] method. The outer black ring represents the cable tunnel where air surrounds the cable. 1) radial heat transfer by conduction within the cable, 2) heat transfer by radiation from the cable surface to the tunnel wall, 3) heat transfer by convection from the cable surface to the air inside the tunnel wall and 4) heat transfer by convection from the air inside the tunnel to the tunnel wall. Lastly, there is a longitudinal heat transfer by convection present, from natural or forced flow of air [1, 17].

The order of the following sections is also the order of calculation of the iterative method, presented in section 2.4.12, which continues until steady air-, cable surface- and tunnel wall temperatures at the outlet are achieved.

2.4.2 Radiation Heat Transfer from the Cable Surface to the Tunnel Wall

In Figure 2.7, the radiation heat transfer from the cable surface to the tunnel wall is depicted as (2) and modeled by T_{st} which is the radiation thermal resistance between the power cable and the tunnel wall and is given by

$$T_{st} = \frac{1}{\pi \cdot D_e \cdot K_t \cdot K_r \cdot \sigma_b \cdot [(\theta_s(L) + 273)^2]} \cdot \frac{1}{[(\theta_s(L) + 273) + (\theta_t(L) + 273)]}, \quad [\mathrm{K\,m\,W^{-1}}] \quad (7)$$

where D_e is the diameter of the cable [m], σ_b is Stefan-Boltzmann constant and $\theta_s(L)$ and $\theta_t(L)$ are cable surface and tunnel inner surface temperatures at the tunnel outlet [°C]. Furthermore, K_t is the emissivity of the cable surface, which is usually 0.9 for cables with outer sheaths and K_r is the radiation shape factor and can be calculated using

$$K_r = \frac{1 - F_m}{1 - (1 - K_t) \cdot F_m}, \tag{8}$$

where F_m is a coefficient that is given in Table 1 in IEC 60287-2-3[1] [1].

2.4.3 Convectional Heat Transfer from the Cable Surface to the Air Inside the Tunnel

In Figure 2.7 the convection thermal resistance is shown as (3) and can be calculated using

$$T_{as} = \frac{1}{\left[\pi \cdot D_e \cdot h - \frac{1}{30^{1/4} \cdot T_{st}}\right] \cdot [\theta_s(L) - \theta_{at}(L)]^{1/4}}. \qquad [\mathrm{K\,m\,W^{-1}}] \tag{9}$$

Equation 9 is valid as long as the Reynolds number is below 2000. Furthermore, h is the heat dissipation coefficient for cables in still air, which can be calculated using

$$h = \frac{Z}{{D_e}^g + E}, \qquad [\mathrm{W/m^2K^{5/4}}] \tag{10}$$

where Z, E and g are constants given in Table 2 in IEC 60287-2-1[3] [30]. Furthermore $\theta_{at}(L)$ is the air temperature at the tunnel outlet in [°C].

If the Reynolds number were to be higher, indicating turbulent flow, the convection thermal resistance shall be calculated using

$$T_{as} = \frac{1}{\pi \cdot k_{air} \cdot K_{cv} \cdot Re^{0.65}}, \qquad [\mathrm{K\,m\,W^{-1}}] \tag{11}$$

where Reynolds number is defined as

$$R_e = \frac{V \cdot D_e}{\nu}. \tag{12}$$

For equation 12, V is the velocity of air in $[\mathrm{m\,s^{-1}}]$ and D_e is the cable diameter in [m]. Additionally, ν is the kinematic viscosity of air and is calculated by

$$\nu = 1.32 \cdot 10^{-5} + 9.5 \cdot 10^{-8} \cdot \theta_{at}(L), \qquad [\mathrm{m^2\,s^{-1}}] \tag{13}$$

and k_{air} is the thermal conductivity for air and is defined as

$$k_{air} = 2.42 \cdot 10^{-2} + 7.2 \cdot 10^{-5} \cdot \theta_{at}(L). \qquad [\mathrm{W\,m^{-1}\,K^{-1}}] \tag{14}$$

Finally, K_{cv} is a constant that is experimentally derived and the value is given in Table 2 in IEC 60281-2-3[1] [1].

2.4.4 Convectional Heat Transfer from the Air Inside the Tunnel to the Inner Tunnel Wall

The convectional heat transfer from the air to the inner tunnel wall, labelled as (4) in Figure 2.7, can be represented by the convectional thermal resistance between the air and the inner tunnel wall and is given as

$$T_{at} = \frac{1}{\pi \cdot k_{air} \cdot 0.023 \cdot R_e^{0.8} \cdot P_r^{0.4}}, \qquad [\mathrm{K\,m\,W^{-1}}] \quad (15)$$

which is valid for Reynolds numbers larger than 2500, i.e. when the air flow is turbulent. The Reynolds number for this equation is given as

$$R_e = \frac{V \cdot D_t}{\nu}, \quad (16)$$

where D_t is the inner diameter of the tunnel given in [m]. In equation 15, P_r is defined as

$$P_r = C_{pair} \cdot \frac{\nu}{k_{air}}, \quad (17)$$

and C_{pair} is the specific heat of air per unit volume and is calculated using

$$C_{pair} = P_r \cdot \frac{\nu}{k_{air}}, \qquad [\mathrm{J\,m^{-3}\,K^{-1}}] \quad (18)$$

where the Prandtl number in this case is

$$P_r = 0.715 - (2.5 \cdot 10^{-4} \cdot \theta_{at}(L)). \quad (19)$$

The convectional thermal resistance between the air and the inner tunnel wall T_{at} can be neglected for Reynolds numbers lower than 2500, i.e. when the air flow is laminar.

2.4.5 Convectional Heat Transfer in Longitudinal Direction

To describe the longitudinal heat transfer by convection, as a result of natural or forced flow of air inside the tunnel, the specific heat of air is needed and is defined as

$$C_{av} = C_{pair} \cdot V \cdot A_t, \qquad [\mathrm{W\,K^{-1}}] \quad (20)$$

where A_t is the inner cross-sectional area of the tunnel in [$\mathrm{m^2}$] [1].

2.4.6 Heat Conduction in the Surrounding Soil in Radial Direction

Finally, the heat dissipates radially in all directions in the surrounding soil. This thermal resistance of the external surrounding of the cable tunnel can, for circular tunnels, be expressed as

$$T_e = \frac{\rho_{soil}}{2 \cdot \pi} \cdot \ln\left(\mu + \sqrt{\mu^2 - 1}\right), \qquad [\mathrm{K\,m\,W^{-1}}] \quad (21)$$

where μ is calculated by

$$\mu = \frac{2 \cdot L_t}{D_t}. \quad (22)$$

In equation 21, ρ_{soil} is the thermal resistivity of the soil in $[\mathrm{K\,m\,W^{-1}}]$ and for equation 22, L_t is the depth of the center of the tunnel in [m] [1].

2.4.7 Cable External Thermal Resistances

The thermal resistance of the cable can be expressed as

$$T_s = \frac{(T_{st}/N_c) \cdot (T_{as}/N_c)}{(T_{st}/N_c) + (T_{as}/N_c) + T_{at}}, \qquad [\mathrm{K\,m\,W^{-1}}] \quad (23)$$

where N_c is the number of cables in operation. Additionally the thermal resistance of the tunnel wall and the thermal resistance of air can be calculated using the following two equations [1],

$$T_t = \frac{(T_{at}) \cdot (T_{st}/N_c)}{(T_{st}/N_c) + (T_{as}/N_c) + T_{at}}, \qquad [\mathrm{K\,m\,W^{-1}}] \quad (24)$$

$$T_a = \frac{(T_{at}) \cdot (T_{as}/N_c)}{(T_{st}/N_c) + (T_{as}/N_c) + T_{at}}. \qquad [\mathrm{K\,m\,W^{-1}}] \quad (25)$$

2.4.8 Cable Internal Thermal Resistances

Subsequently, the thermal resistance per core between the conductor and the sheath is given by

$$T_1 = \frac{\rho_T}{2\pi} \cdot ln\left[1 + \frac{2t_1}{d_c}\right], \qquad [\mathrm{K\,m\,W^{-1}}] \quad (26)$$

where ρ_T is the thermal resistivity of the insulation in $[\mathrm{K\,m\,W^{-1}}]$, d_c is the diameter of the conductor in [mm] and t_1 is the thickness of the insulation between conductor and sheath in [mm]. In addition, the thermal resistance of the outer sheath is defined as

$$T_3 = \frac{\rho_T}{2\pi} \cdot ln\left[1 + \frac{2t_3}{D'_a}\right], \qquad [\mathrm{K\,m\,W^{-1}}] \quad (27)$$

for which t_3 is the thickness of the outer sheath in [mm] and D'_a is the external diameter of the sheath in [mm] [30].

2.4.9 Solving for the Permissible Current Rating

The ampacity of the cable is obtained using

$$I = \left[\frac{\theta_{max} - [\theta_a + \Delta\theta_0] - W_d \cdot \left[\frac{T_1}{2} + n \cdot (T_2 + T_3 + T_{4t}) \right]}{R \cdot [T_1 + n \cdot (1 + \lambda_1) \cdot T_2 + n \cdot (1 + \lambda_1 + \lambda_2) \cdot (T_3 + T_{4t})]} \right]^{1/2}. \quad [\text{A}] \quad (28)$$

In equation 28, θ_a is the ambient temperature at ground level in [°C] and R is the AC resistance of the conductor in [Ω] at maximum operating temperature. Furthermore, T_2 is the thermal resistance between sheath and armour and $\Delta\theta_0$ is the fictitious increase of ambient temperature as a direct result of the ventilation, measured in [K] and is defined as

$$\Delta\theta_0 = [\theta_{at}(0) - \theta_a] \cdot \frac{T_t + T_e}{T_a + T_t + T_e} \cdot e^{-L/L_0}. \quad [°\text{C}] \quad (29)$$

$\theta_{at}(0)$ is the air temperature at the tunnel inlet in [°C] and L_0 is a reference length, given in [m], and can be calculated using

$$L_0 = (T_a + T_t + T_e) \cdot C_{av}. \quad [\text{m}] \quad (30)$$

The equivalent thermal resistance of the medium surrounding the cable is described by

$$T_{4t} = N_c \cdot \left[T_s + (T_t + T_e) \cdot 1 - \frac{T_t + T_e}{T_a + T_t + T_e} \cdot e^{-L/L_0} \right]. \quad [\text{K m W}^{-1}] \quad (31)$$

The dielectric losses per length of cable is given by

$$W_d = \omega \cdot C \cdot U_o^2 \cdot tan(\delta), \quad [\text{W m}^{-1}] \quad (32)$$

where ω is the angular frequency given in equation 36, C is the capacitance per length of cable in [F m^{-1}] and U_0 is the voltage to earth in [V].

Lastly, θ_{max} is the maximum conductor temperature in [°C] that can be allowed to maintain the insulation quality of the power cable over time.

2.4.10 Power Losses in Sheath and Armour

In equation 28, λ_1 is a power loss factor for the sheath and is expressed as

$$\lambda_1 = \lambda_1' + \lambda_1'', \quad (33)$$

where λ_1' are the losses produced by circulating currents and λ_1'' are the losses caused by eddy currents. The losses produced by circulating currents can be calculated using the

following equation:

$$\lambda_1' = \frac{R_s}{R} \frac{1}{1 + \left(\frac{R_s}{X}\right)^2}, \tag{34}$$

where R_s is the resistance of the sheath per unit length at the maximum operating temperature of the cable and is given in $[\Omega\,\mathrm{m}^{-1}]$. Equation 34 is valid for single core cables in trefoil formation with sheaths bonded at both ends. X is the reactance of the sheath per unit length of cable and is represented by

$$X = 2 \cdot \omega \cdot 10^{-7} \cdot \ln\left(\frac{2s}{d}\right), \qquad [\Omega\,\mathrm{m}^{-1}] \tag{35}$$

where s is the distance between the conductor axes in [mm] and d is the average diameter of the sheath in [mm]. ω is the angular frequency and is defined as

$$\omega = 2 \cdot \pi \cdot f. \qquad [\mathrm{s}^{-1}] \tag{36}$$

Furthermore, for large conductors of insulated segmented construction, such as a Milliken conductor, the eddy current loss factor can not be ignored and is calculated using

$$\lambda_1'' = \lambda_1'' \cdot F, \tag{37}$$

where the sheath loss is multiplied by a factor F defined as

$$F = \frac{4 \cdot M^2 \cdot N^2 + (M+N)^2}{4 \cdot (M^2+1) \cdot (N^2+1)}, \tag{38}$$

where, for cables in trefoil formation, the coefficients M and N are represented by

$$M = N = \frac{R_s}{X}. \tag{39}$$

Additionally, the eddy-current losses for single-core cables with single point bonded sheaths or cross-bonded sheaths, the loss factor is represented by

$$\lambda_1'' = \frac{R_s}{R} \cdot \left[g_s \cdot \lambda_0 \cdot (1 + \Delta_1 + \Delta_2) + \frac{(\beta_1 \cdot t_s)^4}{12 \cdot 10^{12}} \right]. \tag{40}$$

For equation 40, the coefficients g_s and β_1 are given by the following equations:

$$g_s = 1 + \left(\frac{t_s}{D_a}\right)^{1.74} \cdot (\beta_1 \cdot D_a \cdot 10^{-3} - 1.6), \tag{41}$$

$$\beta_1 = \sqrt{\frac{4 \cdot \pi \cdot \omega}{10^7 \cdot \rho_S}}. \tag{42}$$

In equation 42, ρ_S is the resistivity of the sheath at operating temperature in [$\mathrm{K\,m\,W^{-1}}$], D_a is the external diameter of the cable sheath in [mm] and t_s is the thickness of the sheath in [mm].

Finally, for three single-core cables in trefoil formation the coefficient

$$\lambda_0 = 3 \cdot \left(\frac{m^2}{1+m^2} \right) \cdot \left(\frac{d}{2s}^2 \right), \tag{43}$$

where s is the distance between the center axes of the conductors in [mm] and m is given by

$$m = \frac{\omega}{R_s} \cdot 10^{-7}. \tag{44}$$

The coefficient Δ_1 is defined as

$$\Delta_1 = (1.14 \cdot m^{2.45} + 0.33) \cdot \left(\frac{d}{2s} \right)^{(0.92 \cdot m + 1.66)}. \tag{45}$$

Furthermore, the coefficient Δ_2 can be neglected for trefoil formation. This holds true unless the value of m is less than or equal to 0.1 whereas both Δ_1 and Δ_2 can be neglected. The ratio of the total losses in the armour to the total conductor losses, λ_2, in equation 28 can be neglected when the power cable does not have armouring.

2.4.11 Air-, Cable Surface- and Tunnel Wall Temperatures

The temperature at the tunnel outlet is approximated using

$$\theta_{at}(L) = \theta_{at}(0) + [\theta_a + (T_t + T_e) \cdot N_c \cdot W_k - \theta_{at}(0)] \cdot \left[1 - e^{-\frac{L}{L_0}} \right]. \quad [^\circ\mathrm{C}] \tag{46}$$

Furthermore, the surface temperature of the cable and the tunnel outlet wall temperature is derived from equation 46 and are given by

$$\theta_s(L) = \theta_{at}(L) + T_a \cdot W_a(L) + T_s \cdot N_c \cdot W_k, \quad [^\circ\mathrm{C}] \tag{47}$$

$$\theta_t(L) = \theta_{at}(L) + T_a \cdot W_a(L) - T_t \cdot [N_c \cdot W_k - W_a(L)]. \quad [^\circ\mathrm{C}] \tag{48}$$

In equation 47 and 48, $W_a(L)$ is the heat extracted by the air at the tunnel outlet and is defined as

$$W_a(L) = \frac{(T_t + T_e) \cdot N_c \cdot W_k - [\theta_{at}(L) - \theta_a]}{T_a + T_t + T_e}. \quad [\mathrm{W\,m^{-1}}] \tag{49}$$

The total heat generated by the cable is used in equations 46, 47, 48 and 49 and is represented by

$$W_k = n \cdot [W_c \cdot (1 + \lambda_1 + \lambda_2) + W_d], \quad [\mathrm{W\,m^{-1}}] \tag{50}$$

where W_c are the losses in the conductor when operating at maximum conductor temperature and is given by

$$W_c = R \cdot I^2. \qquad [\mathrm{W\,m^{-1}}] \quad (51)$$

2.4.12 Iteration Procedure

The equations stated above are used in an iterative process in order to calculate the permissible current rating. As a first estimate, the cable surface temperature $\theta_s(L)$ (equation: 47), the tunnel wall temperature $\theta_t(L)$ (equation: 48) and the air temperature $\theta_{at}(L)$ (equation: 46) at the tunnel outlet are set to be equal to the temperatures at the tunnel inlet. The thermal resistances of the cable (T_s), tunnel wall (T_t) and air (T_a) are then calculated using equations 23, 24 and 25.

The cable permissible current can subsequently be obtained using equation 28. Furthermore, the losses of the power cable, W_k and W_c, are calculated by usage of equations 50 and 51.

The air temperature $\theta_{at}(L)$ (equation: 46) and the cable surface temperature $\theta_s(L)$ (equation: 47) as well as the tunnel wall temperature $\theta_t(L)$ (equation: 48) at the tunnel outlet are again calculated with the updated variables. This procedure continues, with the new estimations of the temperatures at the tunnel outlet, until the temperatures converge to a degree set by ϵ, given in Table 2.

The iteration process, as a flow chart, is shown in Figure 2.8.

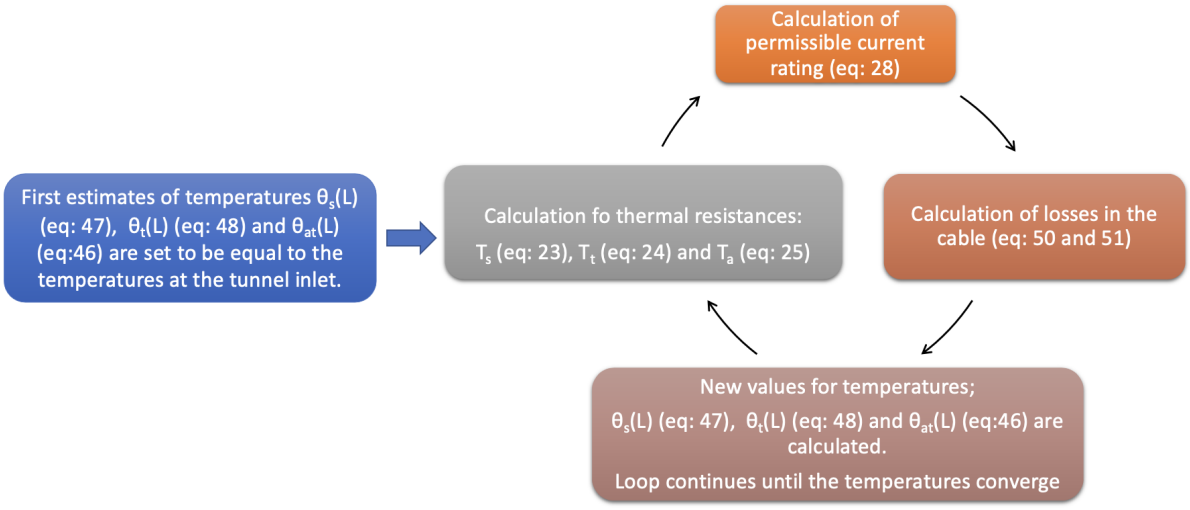

Figure 2.8: Visualization of the iterative process in the IEC 60287-2-3[1] method.

2.5 Thesis Case Background

The power cables subject of this study are owned by a large scale distribution grid operator in Norway called Lede. The location of the site is undisclosed due to confidentiality. The

power cable is laid in a bore hole which is situated underground in mountainous conditions with an incline of 22.3 %, shown in Figure 2.9. The bore hole starts at a height above sea level of 78.80 m and ends at 27.76 m above sea level. The hole is 235.6 m long and has a diameter of 600 mm. The depth of the tunnel is set to be 24 m below the mountainous terrain above. When calculations are made the worst possible thermal scenario is used to ensure safe operation and that is why the deepest depth of Figure 2.9 is used.

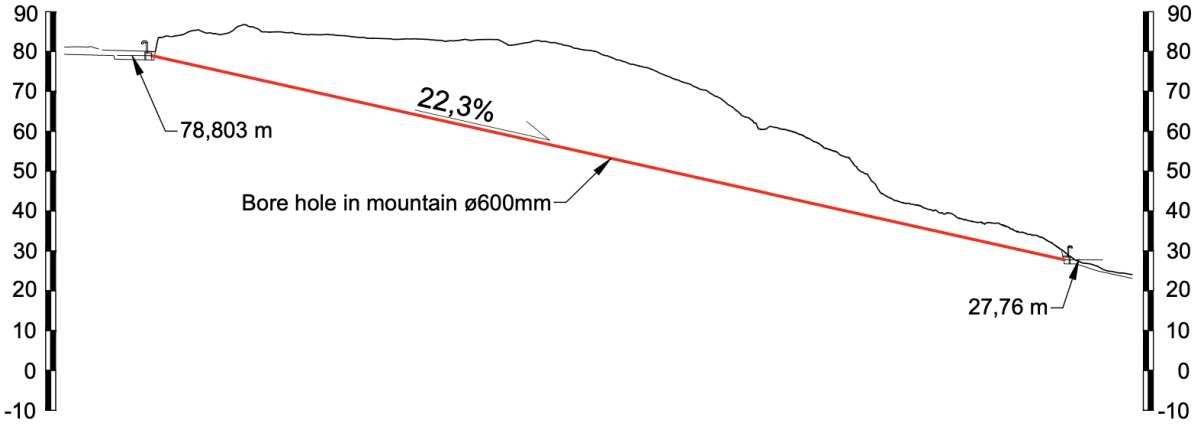

Figure 2.9: Side view of the bore hole through the mountain. Scale is 1:500. Bore hole has a length of 235.6 m sloping 22.3 %. Basins with goose neck ventilation can be seen at the start and end of the tunnel. Reproduced with permission from Lede [31].

There are four cables in the tunnel, one for each phase in addition to a reserve phase cable. The placement of the four phases in the tunnel is depicted in Figure 2.10.

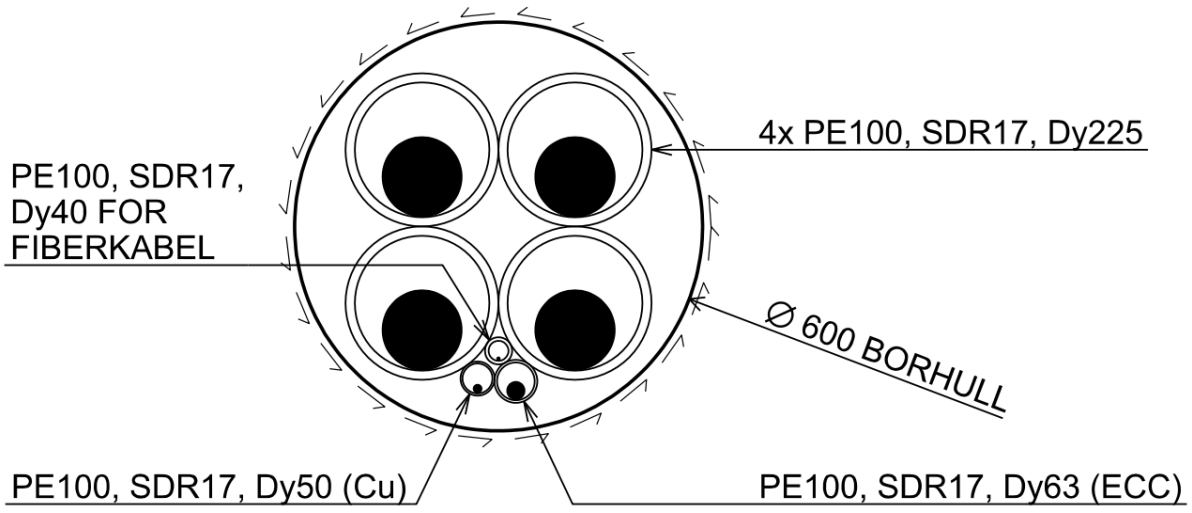

Figure 2.10: Bore hole with a diameter of 600 mm, containing pipes of PE100, SDR17 quality of diameter 225 mm, 63 mm, 50 mm and 40 mm. The pipes contain, in order, conductor, ECC, copper earthing and fiber optics for temperature measurements. Reproduced with permission from Lede [31].

The conductors, the copper earthing, the earth continuity conductor (ECC) and the DTS-fiber are all laid in PE100 pipes which have an SDR17 thickness and are of various diameters [31].

PE100 is a rating for polyethylene pipes which states that the pipes have been certified to withstand a minimum required strength (MRS) test. The MRS rating for PE100 is at a pressure of 10 MPa at 20 °C for 50 years [32]. A prediction of the MRS for a 50 year design lifetime is done by extrapolating the test data obtained over a shorter time span [33]. Furthermore the standard dimension ratio (SDR) is defined as the ratio between the outside diameter of the pipe and the wall thickness [34].

One of the phases and the reserve phase has DTS-fiber optics for temperature surveillance. The individual cables are rated at a 132 kV operating voltage. The conductor area is 2000 mm^2 and is made of aluminium. The insulation is made of XLPE and there is a smooth welded aluminium metallic sheath in one of the outer layers. The whole cable is protected by a high density PE outer sheath. The conductors are designed and produced by Iljin electric in Korea [35]. A cut section of the cable is presented in Figure 2.11.

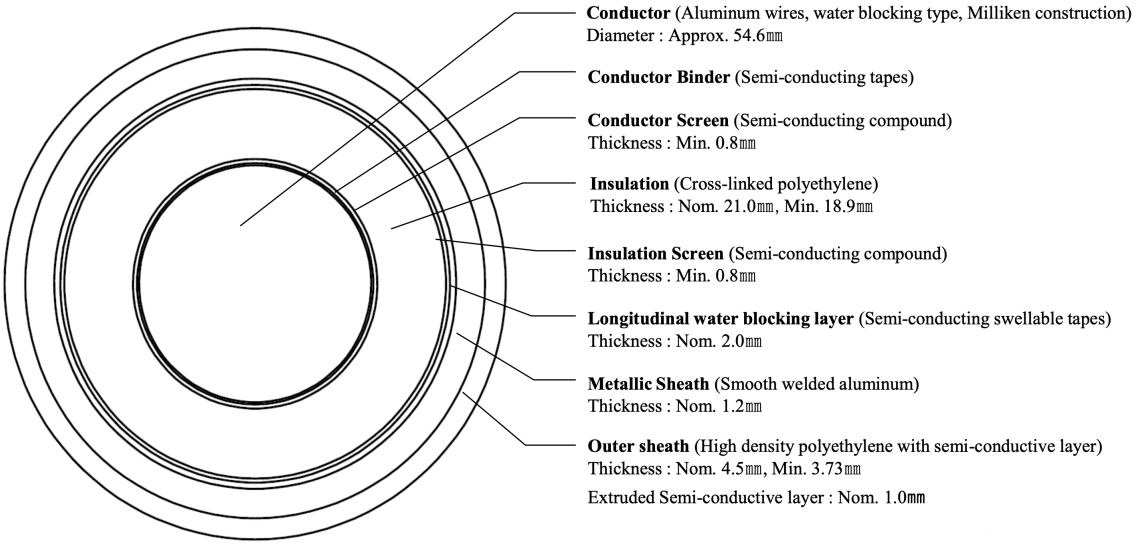

Figure 2.11: 132kV AL/XLPE/Smooth welded AL/PE 2000 mm^2 conductor. Reproduced with permission from Lede [35].

The stated ampacity for this configuration at this site has been calculated by Iljin electric and is 985 A [35].

2.5.1 Data Concerning the Installed Power Cable

The installed power cable at the site provided by Lede has a few electrical and physical properties which are presented in Table 1. The first part of Table 1 concerns properties of the cables in the tunnel, whilst the second part contains information about the physical

properties of the tunnel and its surroundings.

Table 1: Parameters of the power cable site provided by Lede as well as calculated parameters, used in the iterative method [30, 31].

Cable Constants			
	Symbol	**Value**	**Unit**
Number of Cables	N_c	3	-
Number of Conductors in a Cable	n	1	-
Cable Outer Diameter	D_e	0.1224	m
Alternating Current Resistance of the Conductor at its Maximum Operating Temperature	R	$1.9 \cdot 10^{-5}$	Ω/m
Maximum Permissible Conductor Temperature	θ_{max}	90	°C
Thermal Resistivity of the Insulation	ρ_t	3.5	K·m/W
Diameter of Conductor	D_c	54.6	mm
Thickness of Insulation between Conductor and Sheath	t_1	21	mm
Thickness of the Outer Sheath	t_3	4.5	mm
External Diameter of the Metallic Sheath	D_a	106.2	mm
Maximum Capacitance per Meter	C	$2.6 \cdot 10^{-10}$	F/m
Voltage to Earth	U_0	$76 \cdot 10^3$	V
Loss Factor for the Insulation	$tan(\delta)$	0.001	-
Distance between Conductor Axes	s	230	mm
Resistance of Sheath per Unit Length	R_s	0.00335	Ω/m
Mean Diameter of the Sheath	d	106.2	mm
Reactance per Unit Length of the Sheath	X	$9.21 \cdot 10^{-5}$	Ω/m
Electrical Resistivity of Aluminum Sheath at Operating Temperature	ρ_s	$2.8 \cdot 10^{-8}$	Ωm
Thickness of Sheath	t_s	1.2	mm
Tunnel and Site Specifications			
Soil Thermal Resistivity	ρ_{soil}	1	K·m/W
Depth of Tunnel Axis	L_t	24	m
Inner Diameter of the Tunnel	D_t	0.6	m
Inner Cross Sectional Area of the Tunnel	A_t	0.283	m
Length of Tunnel	L	235.6	m

Table 2, firstly contains constants which have been derived from equations in section 2.4. The second part presents the thermal resistances needed for calculating the ampacity of the cable and the final part of the table contains the losses present in the cables.

Table 2: Constants and losses used in the iterative calculation [1, 13].

Convergence Limit for Iterative Process	ϵ	10^{-5}	-
Constants Derived from Equations			
Convection Factor for Trefoil Formation	K_{cv}	0.070	-
Radiation Coefficient for Three Cables Touching	F_m	0.363	-
Effective Emissivity	K_t	0.9	-
Radiation Shape Factor	K_r	0.661	-
Heat Dissipation Coefficient	h	51.05	$\mathrm{W/m^2{\cdot}K^{5/4}}$
Thermal Resistances			
Thermal Resistance per Core between Conductor and Sheath	T_1	0.318	K·m/W
Thermal Resistance between Sheath and Armour	T_2	0	K·m/W
Thermal Resistance of Outer Sheath	T_3	0.045	K·m/W
Losses			
Dielectric Losses	W_d	0.472	W/m
Ratio of Losses in the Sheath by Circulating Currents to the Losses in the Conductor	λ_1'	0.130	-
Ratio of Losses in the Sheath by Eddy Currents to the Losses in the Conductor	λ_1''	0.00815	-
Ratio of Total Losses in the Sheath to the Total Losses in the Conductor	λ_1	0.138	-
Ratio of Total Losses in the Armour to the Total Conductor Losses	λ_2	0	-

3 Literature Review

During this dissertation proceeding, various articles have been assessed. However, there are few articles written on the topic of cable ampacity in ventilated tunnels. This section provides insight into a few of the main findings to gain a broader understanding of the value and challenges of natural ventilation in power cable tunnels.

3.1 Ventilated Power Cable Tunnels

In a paper by George J. Anders and Heinrich Brackelmann [9], it was shown that a significant increase in cable ampacity could be achieved by adding ventilated pipes that interact with the outside air. The paper presents a case where air-filled pipes are connected to a cable tunnel at the ends of the route and led to the surface to interact with the outside air. The temperature differences along the cable route leads to a self propelling air convection which provides cool air for the cable. For longer distances, defined as kilometer long tunnels, forced ventilation can be added for improved cooling effect. The two ventilation pipes are of different length which houses two vertical columns of air with dissimilar temperatures. The non-identical temperatures gives rise to different air densities and results in an air movement with relatively constant velocity [9]. Due to thermal effects, the cooling pipes will continue to circulate the outside air as long as the air temperature is lower than the ambient soil temperature at the pipe opening [9].

The paper also presents an example with a 110 kV cable with a 1000 mm^2 Milliken copper conductor. The cable tunnel was laid one meter underground in a 33 m long pipe and it was calculated that a natural wind velocity of 0.81 $m\,s^{-1}$ was achieved with a soil temperature of 20 °C and an inlet air temperature of 25 °C. Furthermore, the outlet air temperature was assumed to be 40 °C that resulted in a mean air temperature of the pipe of 33 °C [9].

One other interesting point made by the authors of the paper is that adding a fan, for active cooling, does not necessarily mean adding an additional power source to power the fan with. Induction conductors can be connected to a coil which is laid in parallel to the power cable. By induction, a voltage and current will be induced in the coil by the alternating current of the main power cable, hence powering the fan. The amount of air flow provided by the fan will also be directly proportional to the load of the power cable [9].

3.2 Air Filled Culverts With and Without Pipe Installation

A project by Heggås [36] performed COMSOL simulations to evaluate the operating conductor temperature for various underground environments. This was done for a subsea power cable route. A shore section of the cable was buried in an air-filled culvert, with

and without an encapsulating PE pipe. It was shown that by adding a pipe to a cable laid in an air-filled culvert resulted in a higher conductor temperature. The temperature increased from 42 °C to 47.5 °C. These simulations were made for an ambient outside temperature of 20 °C. The encasement of the cable resulted in less natural convection in close proximity of the cable [36].

Further simulations also proved that the ambient temperature had significant impact on the conductor temperature. When the ambient temperature was 0 °C, the conductor temperature of the cable, laid in pipe, dropped from 47.5 °C to 27 °C [36].

This indicates that the conductor temperature is adversely affected by encasement as well as outer temperature.

3.3 Software Model

A software developed by Electrotechnik, ELEK Cable High Voltage™ Software, using the IEC 60287-2-3[1] standard, made an example calculation of the steady-state current rating of a cable installed in a ventilated tunnel [37]. There was 686 A of current going through five trefoil cables at a voltage of 132 kV with a cross-sectional area of 1000 mm^2. The tunnel was 1000 m long with a diameter of 2.2 m, laid at a depth of 2 m. The air velocity in the calculation was varied between 0.5 $m\,s^{-1}$ and 5 $m\,s^{-1}$. The software calculated that the current rating of the cables could be increased from 497.8 A at 0.5 $m\,s^{-1}$ to 907.7 A at 5 $m\,s^{-1}$. The modelling shows that wind inside a cable tunnel can have a significant impact on the permissible current rating of the cable. It was also shown that the length of the tunnel impacted the temperatures of the cables greatly whilst the tunnel depth did not have a noteworthy influence on cable temperatures [37].

4 Materials & Methodology

4.1 Sensors

To obtain data for the comparison between data and the IEC theoretical method, a suite of sensors were installed at the site of the power cable. The sensor, at the bottom location where the air inlet is situated, has a LASCAR EL-USB-2 Temperature USB Data Logger [38]. The specifications for the logger is shown in Table 3.

Table 3: Specifications for the LASCAR EL-USB-2 Temperature USB Data Logger [38].

Measurement Interval	Every 10 minutes
Measurement Range	$-35\,^{\circ}\mathrm{C}$ to $80\,^{\circ}\mathrm{C}$
Internal Resolution	$0.5\,^{\circ}\mathrm{C}$
Accuracy	$\pm\ 0.3\,^{\circ}\mathrm{C}$

At the top basin, a wind sensor coupled with a temperature sensor were mounted. The base unit is a UBIBOT GS1-AL4G1RS Industrial Logger and its specifications are shown in Table 4 [39]. A UBIBOT wind speed logger, with specifications stated in Table 5, was connected to the main unit [40].

Table 4: Specifications for the UBIBOT GS1-AL4G1RS Industrial Logger [39].

Measurement Interval	Every 5 minutes
Temperature	$-20\,^{\circ}\mathrm{C}$ to $60\,^{\circ}\mathrm{C}$
Accuracy	Temperature $\pm\ 0.3\,^{\circ}\mathrm{C}$

Table 5: Specifications for the UBIBOT wind speed logger [40].

Measuring Range	$0\,\mathrm{m\,s^{-1}}$ to $30\,\mathrm{m\,s^{-1}}$
Measurement Accuracy	$\pm(0.3 + 0.03\,\mathrm{V})\ \mathrm{m\,s^{-1}}$, "V" is wind speed
Stabilization Time	<1s
Operating Temperature Range	$-30\,^{\circ}\mathrm{C}$ to $70\,^{\circ}\mathrm{C}$

At the inlet, the LASCAR sensor was installed in such a way that it measured inlet temperature of the cable bore hole. The measurement interval was set to every ten minutes. A schematic view of the bottom sensor mounting is shown in Figure 4.1. Figure 4.2a shows a picture of the sensor mounting solution inside the manhole whilst Figure 4.2b shows an outside view of the manhole.

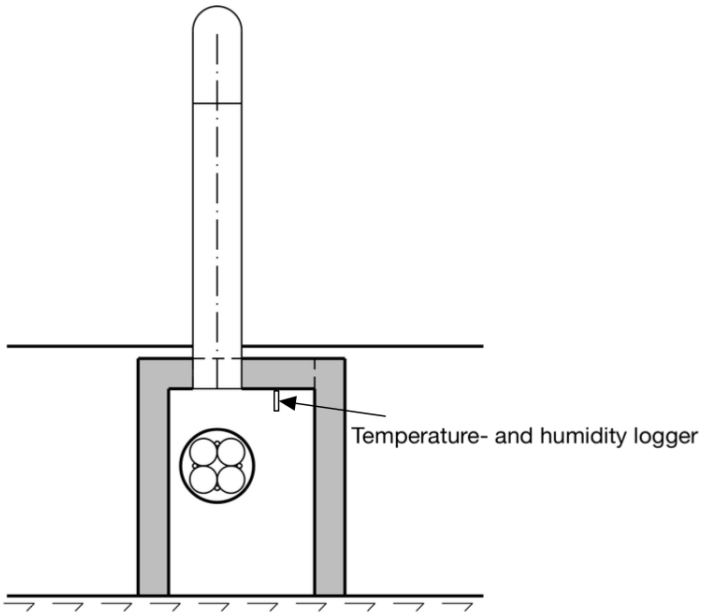

Figure 4.1: Schematic view of mounting placement for the temperature sensor at the air inlet basin. Reproduced with permission from Lede [31].

(a) View of the manhole and the LASCAR EL-USB-2 Temperature USB Data Logger placement.

(b) Outside of the inlet basin with goose neck ventilation inlet and manhole for accessing the logger. The manhole is 600 mm wide.

Figure 4.2: Air inlet sensor mounting location and solution.

At the air outlet basin, the wind sensor and its logger were placed according to Figure 4.3. The wind sensor was mounted in such a way that it was affected by the natural flow of air exiting the top of the bore hole. The logger was placed on the wall next to the wind sensor where it registered temperature. The measuring interval was configured to log data every five minutes. The placement inside the basin of the logger and wind sensor can be seen in Figure 4.4a. A view of the goose neck ventilation pipes fitted at the outlet basin and their grated openings are shown in Figures 4.4b and 4.4c.

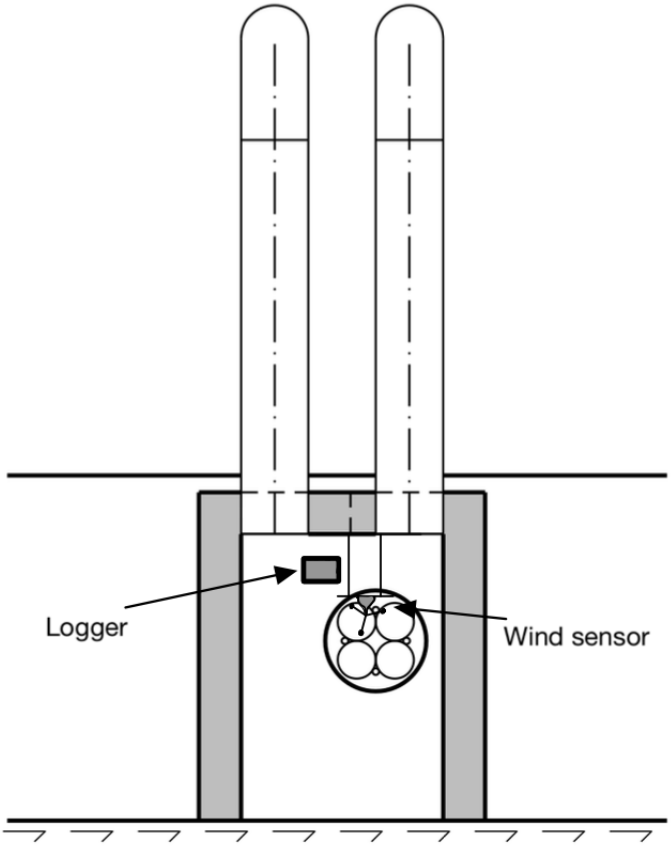

Figure 4.3: Schematic view of the mounting arrangement of the wind sensor and its logger at the air outlet basin. Reproduced with permission from Lede [31].

(a) The mounting bracket and placement of the UBIBOT wind sensor and the UBIBOT GS1-AL4G1RS Industrial Logger at the outlet basin.

(b) Outside of the outlet basin where the two ventilation goose neck pipes are fitted.

(c) View from below of the goose neck gratings which are 400 mm in diameter.

Figure 4.4: Pictures of the air outlet basin and the mounting solution of the sensors.

4.2 Data Processing

The data gathered was timestamped data of the temperature in [°C] and wind speed in [$\mathrm{m\,s^{-1}}$]. The data logging started on the 15$^{\text{th}}$ of December 2022 and lasted until the 15$^{\text{th}}$ of February 2023, resulting in 62 days of logging. Additionally the cable has a DTS-fiber which logs the temperature in [°C]. The logger registers the temperature of one of the phases and the reserve phase for every meter in axial direction. Lastly, load current data of the cable was obtained as a five minute average of the current going through the cable.

The data has been processed using Python. Firstly, the data was merged and grouped into the same ten minute intervals. Subsequently, a smoothing of the data was done, using the Savitzky-Golay method [41]. The filtering was done to gain a greater understanding

of the main tendencies of the data. A flow chart description of the data handling can be observed in Figure 4.5 and the detailed code of the data processing is shown in appendix A.

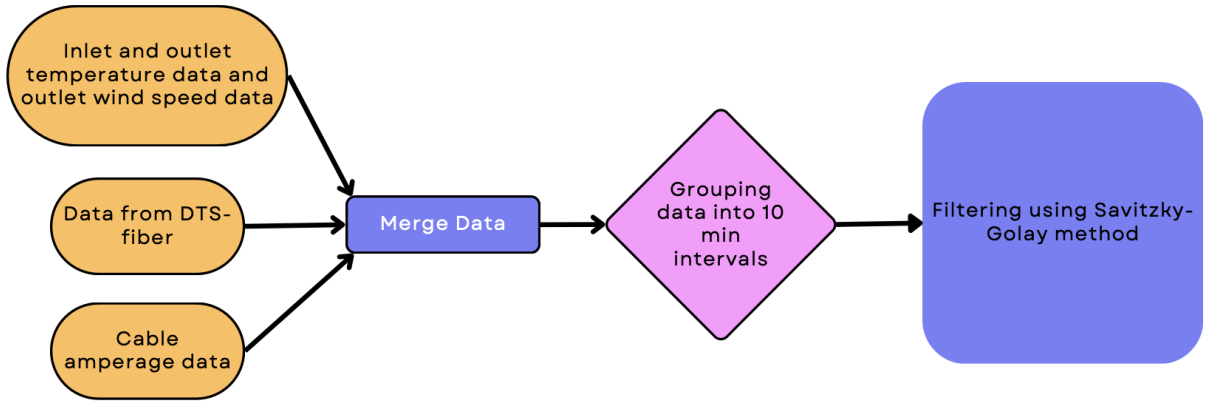

Figure 4.5: Visualization of the data processing approach.

The results will be compared and analyzed to assess whether the theoretical model can be representative of the power cable site presented in this thesis.

4.3 Sources of Error

There are numerous possible sources of discrepancies that have occurred during the process of writing this thesis. The main ones will be presented in this section.

The main issues are inaccuracies regarding especially the wind sensor and its placement. Specifically, the fact that the wind sensor was too big to accurately register the wind coming out of the cable tunnel. A smaller ultrasonic wind sensor would have provided higher accuracy as well as enabled a placement directly in line with the wind flow. Additionally, the temperature sensors and their location inside the basins is also a source of error. This is mainly due to the fact that they were placed too far from the entry and exit point of the cable tunnel as well as the sensors' intrinsic measuring errors.

The model must also be assumed to be conservatively written by the IEC, in order to calculate a safe permissible current rating, which affects the precision of the model in comparison to the collected data. Furthermore, the model is a steady state model whilst the real world system is transient. This adds errors in all calculations made, using the IEC-model. The temperature and thermodynamic properties of the surrounding rock is also not accurately known and can not be quantified by any facile measurements, which leads to further uncertainties within the calculations.

Finally, all data collected in this thesis contains errors following from the intrinsic error properties of the sensors logging the data. The errors of the sensors are stated in section 4.1.

5 Results and Discussion

This section starts by presenting and discussing the results from the modelling of the power cable site provided by the grid power company Lede. The modelling is done using the IEC 60287-2-3[1], IEC 60287-1-1[2] and IEC 60287-2-1 methods[3] [1, 13, 30]. The cable characteristics that are used as a foundation for the modelling in this section are based on the specifications for the cable site provided by Lede, as well as constants derived from equations. These were presented in Tables 1 and 2. The second part of this section will deal with the results from the data collected at the cable tunnel site. This section also presents and analyzes data for the inlet and outlet temperatures as well as outlet wind speed. Data concerning the DTS-fiber will also be presented which includes temperature data for the cable.

5.1 Theoretically Induced Air Velocity

Pressure differences at the outlet and inlet causes a dissimilarity in pressure which induces air flow in the tunnel. The estimation of induced air flow is derived from equation 3 and is presented in Figure 5.1. The figure presents the induced air velocity as a function of air temperature at the outlet for various inlet temperatures. The diameter of the pipe, used for this calculation, is an equivalent diameter. It is calculated using the difference in area between the cable pipe and the conductors obstructing the air flow. This is a modification of the method first presented by George J. Anders [9].

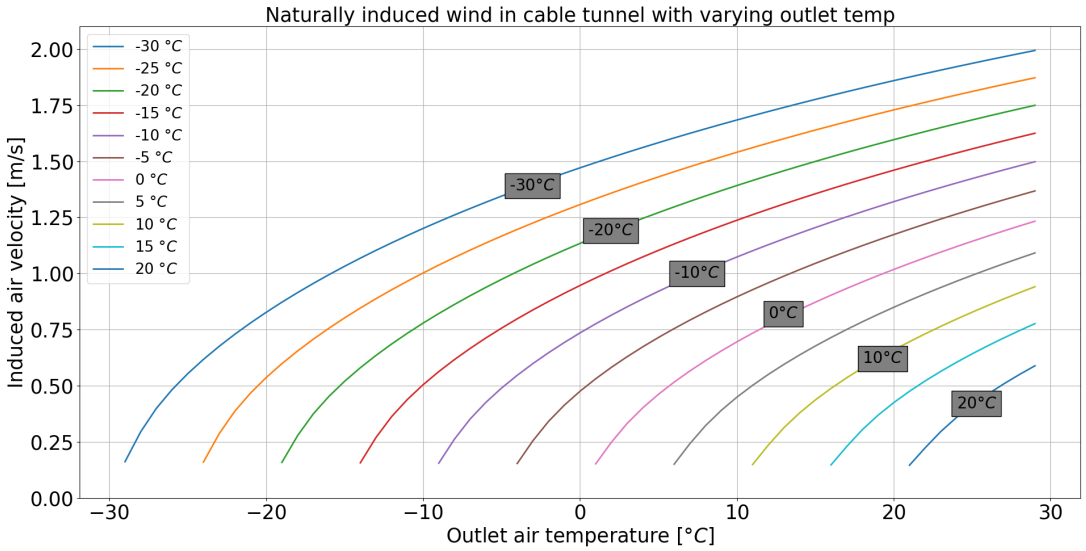

Figure 5.1: The natural air velocity induced by density differences of air with varying inlet and outlet temperatures. The color scheme of the different curves represent the inlet temperature and the x-axis shows various outlet temperatures while the y-axis represents air velocities.

From Figure 5.1, it can be seen that for an inlet temperature of around $-5\,^{\circ}\mathrm{C}$ and an outlet temperature of $6\,^{\circ}\mathrm{C}$, the theoretically induced wind is approximated to $0.7\,\mathrm{m\,s^{-1}}$. These

chosen temperatures are averages from the collected data over the measuring period.

5.2 IEC 60287-2-3 Modelling

By using the iterative method presented in section 2.4.12 and the constants from Table 1 and 2, Figure 5.2 is obtained when varying the natural velocity of air and the outside temperature. The inlet air temperature is set to 0 °C.

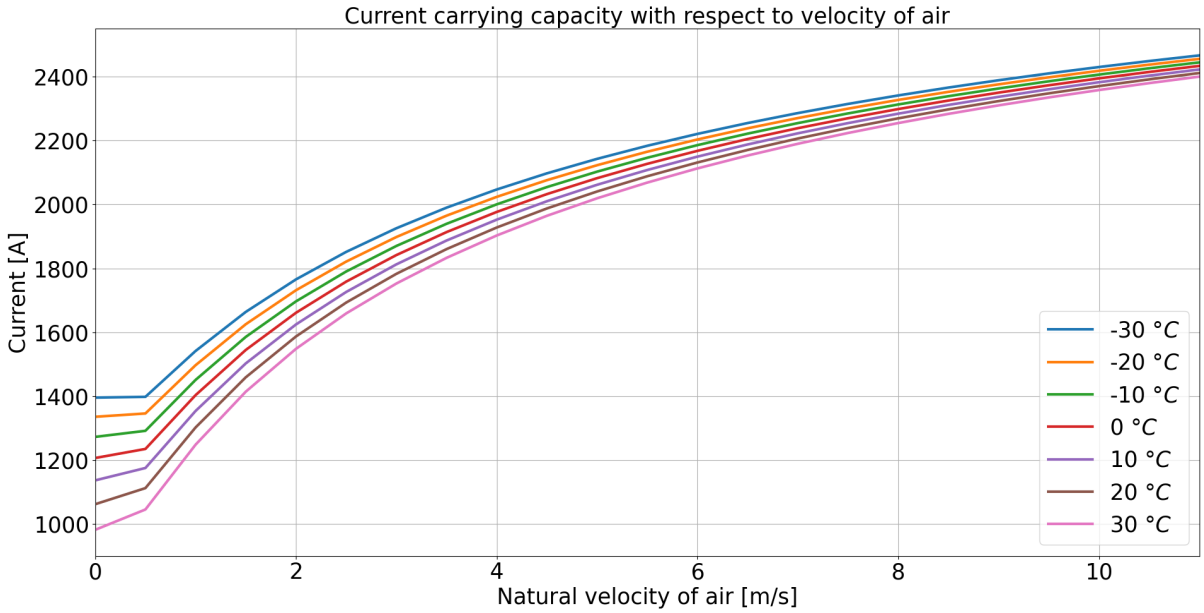

Figure 5.2: Depicts the ampacity rating with varying air velocity and varying outside temperature. The x-axis represents the natural velocity of air whilst the y-axis refers to the permissible current rating. The color scheme represents different outside temperatures in [°C] ranging from negative −30 °C to 30 °C

Figure 5.2 follows an expected pattern, where the ampacity rating increases with the increase in air velocity. The ampacity rating also has an inverse relationship to the outside temperature, i.e. colder temperatures amount to a higher current carrying capacity.

The zero air velocity scenario with an outside temperature of 30 °C results in an ampacity of 981 A. This correlates with the calculated ampacity for the power cable by the cable manufacturer. The calculations made by Iljin electric are based on an ambient temperature of 15 °C, which indicates that the estimates of the manufacturer are on the conservative side. Interpolating for 15 °C in Figure 5.2 gives a rated ampacity of around 1100 A, which is in approximate agreement with the manufacturers estimation when taking into consideration the complex environment of the cable as well as the amount of parameters fed to the model and their possible errors. The amount of safe margin built into the IEC 60287-2-3[1] method is, at the time of writing, unknown. The built in safe margin will also affect the accuracy of the IEC-model in comparison to the results from the cable manufacturer.

The sudden rise in the derivative of the ampacity curves, in Figure 5.2, is largely because of the change in flow characteristics, where the flow goes from laminar to turbulent. The Reynolds number affects which equation is used for the convectional thermal resistance between the cable surface and the air inside the tunnel, described by equation 9 and 11. The convectional thermal resistance between the air and the inner tunnel wall, described by equation 15 is also governed by whether the air flow is laminar or turbulent. In turn, this affects the calculated ampacity rating amounting to the sudden change in the curve.

The cable surface temperature (θ_s) and the air temperature (θ_{at}) at the tunnel outlet can be calculated using equations 47 and 46. This is modelled for varying velocities of natural air movement and with a constant current of 300 A and is presented in Figure 5.3. The inlet temperature (θ_a) is set to 0 °C. The constant current is set to model the average load on the in situ power cable.

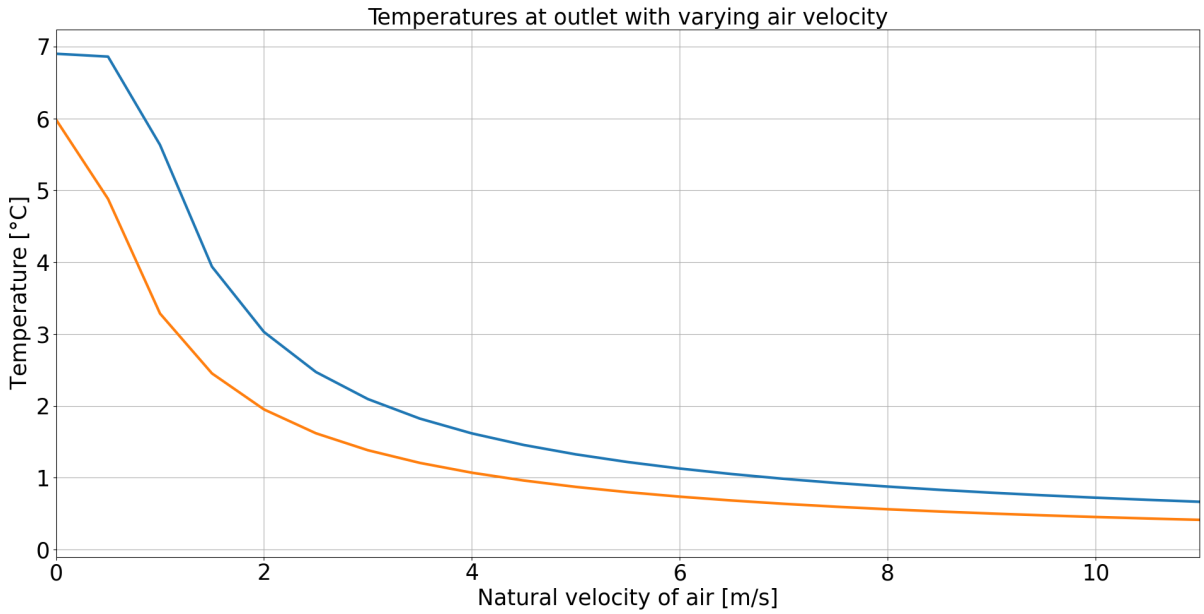

Figure 5.3: (–): Cable surface outlet temperature (θ_s), (–): Air temperature at the outlet (θ_{at}). Plotted with varying air velocity. The plot is made using a constant current of 300 A and an ambient air temperature (θ_a) of 0 °C. The x-axis constitutes the natural velocity of air while the y-axis represents temperatures.

As can be seen in Figure 5.3, the modelled cable temperature as well as the air temperature at the outlet decreases drastically with the increase of air velocity and converges towards the set ambient temperature which is 0 °C. As expected, they follow the same decline pattern where the cable surface temperature is at a slightly elevated level in comparison to the air temperature at the outlet. The biggest decrease in temperature happens within the range between 0 $\mathrm{m\,s^{-1}}$ to 2 $\mathrm{m\,s^{-1}}$, suggesting that low wind speeds have a significant impact on the cable temperature and thus its permissible current rating. This is also verified in Figure 1.2, where the most drastic increase in the heat transfer coefficient

happens within the first $2\,\mathrm{m\,s^{-1}}$. Figure 5.3 also shows that the cable temperature and air temperature at the outlet are low in comparison to the maximum 90 °C that the cable insulation can handle. This emphasizes that the cable is operating at currents at the lower end of what the cable can handle. The effect of the low temperatures and what consequences it has on the data will be prominent in the following paragraphs.

5.3 Sensor Data

As described in section 4.2, the data has been filtered using the Savitzky-Golay method. The filtered and raw data are presented in Figure 5.4. The outlet air temperature has a mean value of around 6 °C, whilst the inlet air temperature has a mean value of −5 °C.

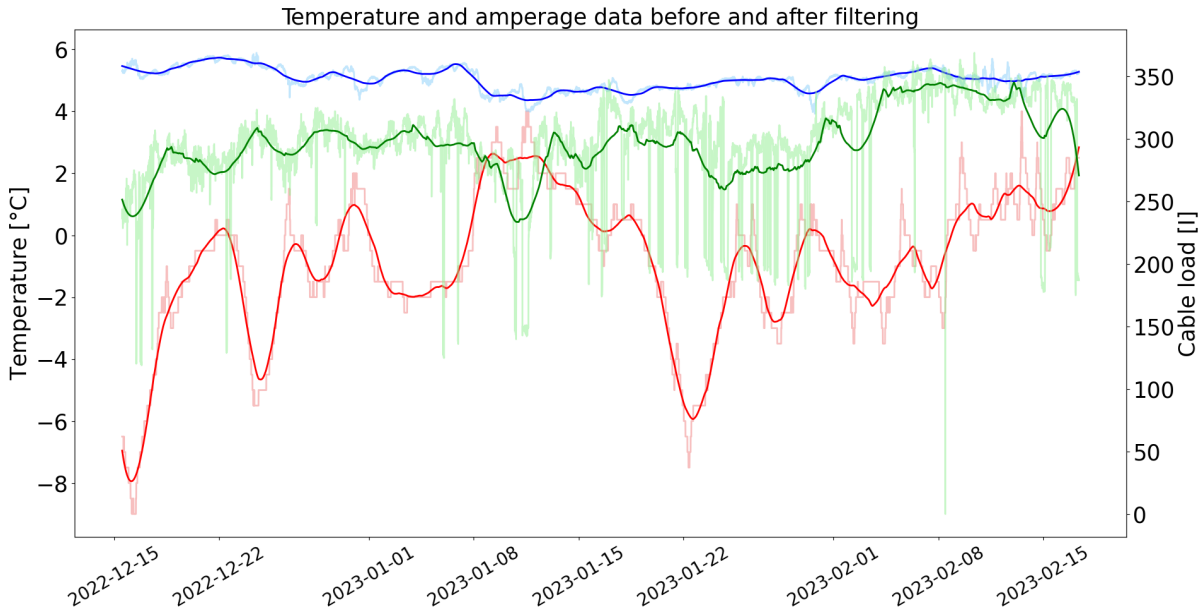

Figure 5.4: (–): Inlet air temperature, (–): Outlet air temperature, (–): Cable load. The lightly colored- and opaque graphs are based on raw data whilst the stronger colors represents data that have been filtered using the Savitzky-Golay method.

Figure 5.4 shows that especially the cable load fluctuates quickly. The sudden variations are mainly due fluctuations in current demand at the receiving end of the cable. The outlet air temperature is kept stable at around 6 °C. The presence of only small fluctuations in the outlet temperature is due to the thermal inertia of the system. The mountain around the bore hole has likely been warmed over time by the cable causing the temperature of the mountain, the bore hole and subsequently the outlet air temperature to remain fairly constant. Additionally, it indicates that the cable load has been kept at around the same values before the measuring period and that the load current has not seen any larger variations over time. Cable temperature data will be further discussed in the last figure of this section.

The outlet air temperature has a low degree of correlation to the inlet air temperature, which again is caused by thermal inertia of the system. The inverted peaks of the inlet air temperature happens during a too short time frame for it to have an effect on the outlet temperature. The cable itself also possesses thermal inertia, which causes the cable to keep a stable temperature in spite of its load current fluctuations. The thermal inertia present in a power cable is exemplified in a master thesis by Heggås. The author performed a COMSOL experiment where a power cable instantaneously went from a full-load condition to a no-load condition. The conductor temperature at the full-load condition was around 38 °C and the conductor needed over 50 hours to cool down to around 15 °C [42]. This underpins the fact that the fluctuations of the cable load current are too quick to have a noticeable impact on the cable temperature. All of these factors subsequently results in the stability of the outlet temperature throughout the measuring period.

Figure 5.5 shows the difference in temperature between the inlet and outlet sensor measurements for the month of December as well as the wind speed from the wind sensor. Cable load current is also included.

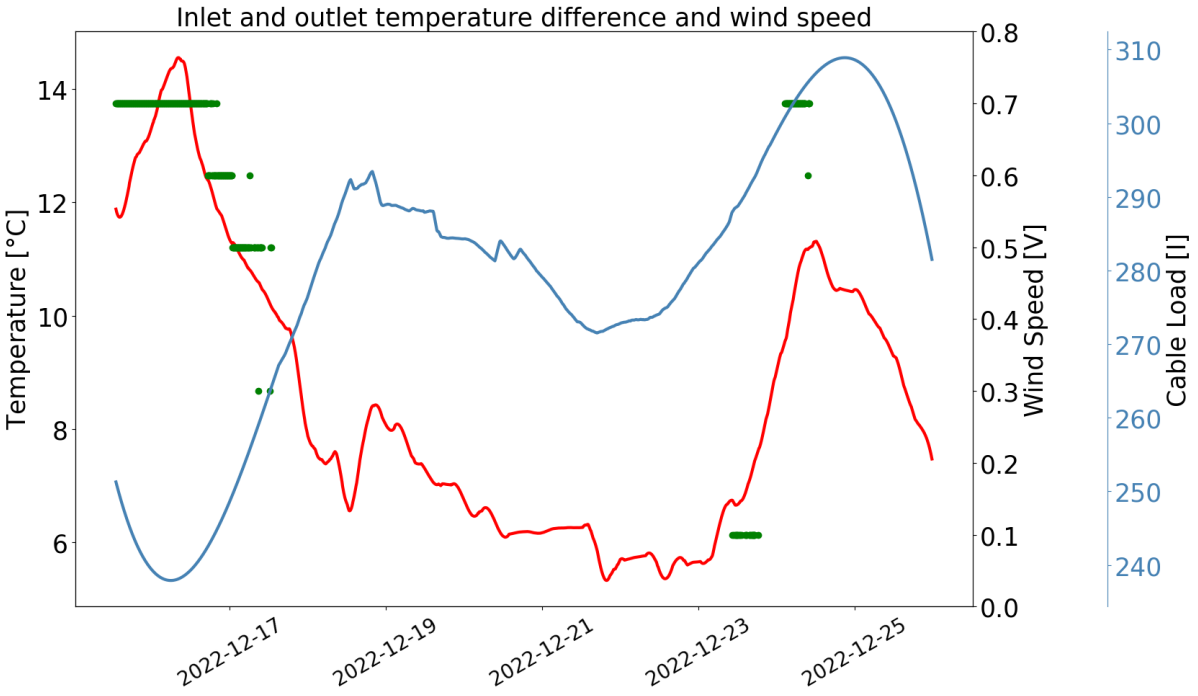

Figure 5.5: (–): Temperature difference between inlet and outlet, (–): Load current of the cable, (o): Wind speed. Data is presented for the month of December. The left y-axis represents temperature whilst the right y-axis represents wind speed and load current. The x-axis constitutes dates over the measuring period.

The thermal inertia of the system can be observed in Figure 5.5. It can be seen that the difference in temperature drops at a delayed point in time from the cable load current, the same is valid for temperature and load current increases. Furthermore, the outlet temperature is kept stable, meaning that the sole reason for change in the temperature

difference is due to the variation in inlet temperature. Cable load and difference in temperature can thus not be considered correlated for this measuring period. Nevertheless, there appears to be a link between the temperature difference and the wind speed peaks. These occur at the same point in time suggesting that larger differences in inlet and outlet temperature gives rise to a more prominent wind speed through the tunnel. This is also what is expected from the modelled wind speed, shown in Figure 5.1.

After the passing of December, no further wind recordings were made and the reason is speculative. It could be due to clogging of the bearings in the wind sensor or due to the fact that the dips in inlet temperature did not last for long enough. The wind sensor placement was neither optimal for the measuring location. The sensor was placed too far away from the pipe outlet to properly represent the outlet temperature. It was also too big to properly cover the tunnel exit. An ultrasonic wind sensor would have been smaller, more accurate and more suitable for the task. Additionally, a more prominent wind speed would have appeared in the tunnel if a larger difference between air temperature at the inlet and outlet would have been present. A higher cable ampacity over a longer time frame would have resulted in this temperature increase. These changes would have allowed more explicit conclusions to be drawn.

The calculated induced wind speed, from Figure 5.1, happens to accurately fit the collected data, which had a top wind speed of $0.7\,\mathrm{m\,s^{-1}}$. Wind speed from data is shown in Figure 5.5. The modification of the induced wind, in equation 3, results in an accurate prediction of the actual wind speed in the pipe for this specific case. However, the amount of wind data that was collected is not enough to draw any strong conclusions about whether an equivalent diameter can be used to model the wind through a cable pipe with cables as wind obstructions. The simplification made, when introducing an equivalent diameter, does not take into account the very complex behaviour of wind and how cables placed in a pipe affects the wind flow. In spite of these drawbacks, the simple approximation presented in this dissertation can be seen as a base for further research and gives a simple and approximative indication of the amount of wind speed that can be expected for cable tunnels.

To evaluate the accuracy of the model, it has been fed data about cable load current, inlet temperature and ambient temperature. The result of the modeled outlet temperature of the system is plotted together with the outlet temperature from the sensor and is shown in Figure 5.6. The MAPE value for the model's accuracy of the outlet temperature is calculated to be ca 20 %.

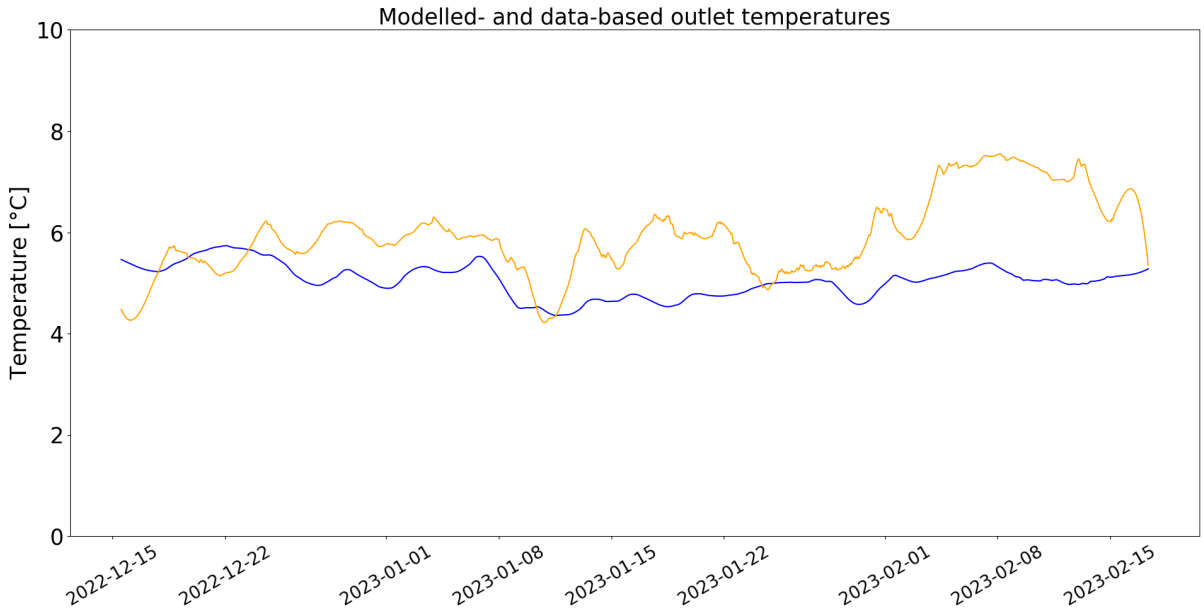

Figure 5.6: (–): Modelled outlet air temperature, (–): Outlet air temperature from sensor-data. The y-axis constitutes the temperature whilst the x-axis represents dates during the measuring period.

The data in Figure 5.6 has been filtered with the Savitzky-Golay method before plotting and calculation of MAPE. The two data sets correlate to a degree described by the MAPE value which was calculated to be ca 20 %. A MAPE value of 20 % means that the data is in good agreement with the model [43]. The reason for the less accurate prediction of the outlet air temperature could be due to the model predicting the outlet air temperature every ten minutes. This is a much faster rate of change in comparison to the thermally slow changes that occur in the power cable and its surroundings. Additionally, the load current fluctuates and for every fluctuation an outlet temperature is calculated. This stand in contrast to the thermal inertia of the in situ cable which results in a stable cable temperature in spite of the varying load current. The cable temperature is shown in Figure 5.7. When taking these arguments under consideration, the model fluctuates at a faster rate than the outlet air temperature collected from the sensor, causing the model to deviate from the sensor temperature. The placement of the outlet air temperature sensor also affects the deviation. The sensor was placed on the inside basin wall at a distance of around one metre from the pipe exit. A sensor placed directly in front of the exit would have obtained more exact temperature measurements, less affected by the temperature of the concrete wall.

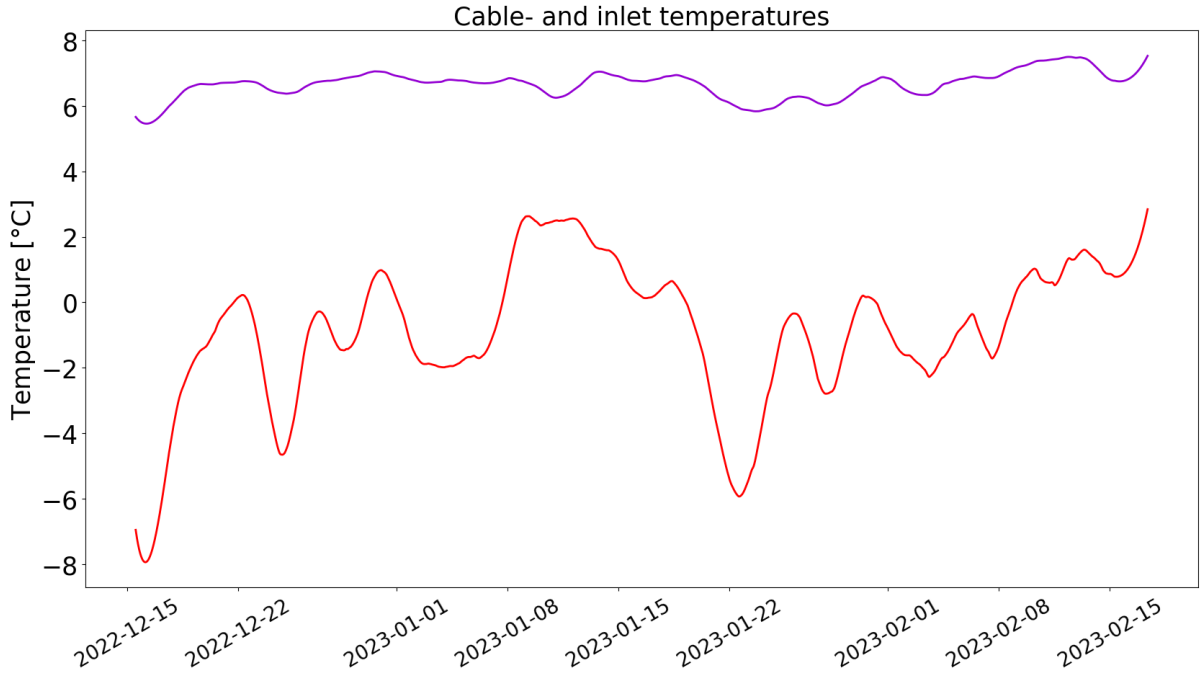

Figure 5.7: (–): Inlet air temperature, (–): Cable temperature from DTS-fiber data. Filtered cable temperature data plotted with data from the inlet temperature sensor.

Figure 5.7 shows Savitzky-Golay filtered data from the DTS-fiber sensor as well as the inlet temperature sensor. The plot shows that the cable temperature is kept at a stable level during the entire measuring period. It is not adversely affected by the change in inlet temperature. This provides a strong corroboration for the fact that the cable possess thermal inertia, making it resistant to change in temperature. The inverse peaks of the inlet temperature do not persist for a long enough duration for it to have an effect on the cable temperature. The deep burial of the cable pipe, also increases the effect of thermal inertia. Rock, situated at depths found at this cable tunnel location, is not affected by the annual fluctuations of the ambient temperature [44]. These findings mean that the cable is kept at a thermally stable environment and that the fluctuations in cable load and ambient temperature are not endured for a long enough period of time to affect the temperature of the power cable. This also helps explain the stable outlet temperature seen in previous graphs.

6 Conclusion

Cable ampacity is an important factor of all cable routes in order to optimize power flow within the grid. This dissertation has delved deeper into the possibility that wind flow in naturally ventilated tunnels can aid in cooling the cable and thus increasing the ampacity rating of the cable. Little has been written on the topic, but the reviewed literature points in the direction of that wind flow will increase the ampacity of a cable tunnel. However, in situ measurement of wind flow in such tunnels have not been widely explored prior to this thesis.

The theoretical model detailed in this paper, based on the IEC 60287-2-3[1] method, shows that the current carrying capacity increases significantly with air flow, as shown in Figure 5.2. The model based on the IEC method has a high degree of correlation with the cable permissible rating obtained from the cable manufacturer when comparing the zero wind scenarios. This suggests that the IEC method, explored in this dissertation, can be used to provide viable predictions of the ampacity rating of an HVAC power cable situated in a naturally ventilated tunnel.

The IEC model was also verified by plotting the modelled outlet temperature with the outlet temperature from data. These correlate to a certain degree described by a MAPE value of ca 20 %, meaning the model is in good agreement with the data. The discrepancy is likely due to quick fluctuations in sensor temperature and cable load, which do not correspond with the thermal inertia of the system. The placement of the sensors has also affected the divergence.

In situ data collection from sensors showed a link between the difference in inlet and outlet temperature and the occurrences of wind inside the tunnel. This indicates that higher delta temperature will result in a stronger wind flow through the tunnel, which corresponds well with the predictions made in this dissertation.

Furthermore, for a system described in this paper with an inlet temperature of $-5\,^{\circ}\mathrm{C}$ and an outlet temperature of around $6\,^{\circ}\mathrm{C}$, the resulting theoretical air flow is around $0.7\,\mathrm{m\,s^{-1}}$. This is obtained from Figure 5.1. The theoretical air flow thus correlates with what was found in the sensor data. This indicates that the method, first proposed by G. J. Anders [10] and with modifications made concerning an equivalent tunnel diameter, can be used to predict wind speed in a cable tunnel. However, predicting the correct wind flow for two measurement occurrences can be shear luck and more wind speed data, over a longer time frame, is needed to draw any explicit conclusions.

Many of the discrepancies in this paper is due to the insufficient difference in inlet and outlet temperatures, resulting from low cable load, as well as an inaccurate wind sensor which was not optimal for the location. The distance, of the temperature sensors from

the actual inlet and outlet, also contributed to the divergences.

Lastly, the power cable site has been found to be thermally stable and that neither the inlet temperature nor the cable load affects the cable temperature or the outlet temperature to a noticeable degree. This is valid for the low load current of the cable encountered during the measurement period. To experience a change in cable temperature and outlet temperature, a higher cable load over time is needed. It is also likely that an increased outlet- and cable temperature would have resulted in more wind speed data.

7 Future Work

The intention of this dissertation was to delve deeper into the workings of air flow inside a cable tunnel and to better understand how air flow affects cable permissible rating. The proceedings of this dissertation also investigated to what extent air flow within the tunnel could be generated from heat stemming from the power cable. A comparison of the findings from sensor data with theoretical calculations was also performed.

Based on the discoveries of this dissertation, the following points are suggested for further research.

- Field work: A new study of a location where the cable load is higher for a longer period of time, resulting in higher cable- and outlet temperatures and more sustained wind speed.
- Repeat measurements with an ultrasonic wind sensor for enhanced placement and accuracy.
- Improved sensor placement, i.e. placing the sensors closer to the start and exit of the cable pipe.
- FEM simulation of the cable site to compare real world data with.

References

[1] International Electrotechnical Commission, "Part 2-3: Cables installed in ventilated tunnels", International Electrotechnical Commission, Standard, 2015. [Online]. Available: https://webstore.iec.ch/publication/28493.

[2] IPCC, "Summary for policymakers", in *Global Warming of 1.5°C: IPCC Special Report on Impacts of Global Warming of 1.5°C above Pre-industrial Levels in Context of Strengthening Response to Climate Change, Sustainable Development, and Efforts to Eradicate Poverty*. Cambridge University Press, 2022, pp. 1–24. DOI: 10.1017/9781009157940.001.

[3] R. Shukla *et al.*, "Summary for Policymakers", *Climate Change 2022: Mitigation of Climate Change. Contribution of Working Group III to the Sixth Assessment Report of the Intergovernmental Panel on Climate Change*, 2022. DOI: 10.1017/9781009157926.001. [Online]. Available: https://www.ipcc.ch/report/ar6/wg3/downloads/report/IPCC_AR6_WGIII_SummaryForPolicymakers.pdf.

[4] NHO, "Verden og oss næringslivets perspektivmelding 2018", *Næringslivets Hovedorganisasjon*, 2018, (Accessed on 01/18/2023). [Online]. Available: https://www.nho.no/siteassets/publikasjoner/naringslivets-perspektivmelding/pdf-er-30okt18/nho_perspektivmeldingen_hele_web_lowres.pdf.

[5] U. Nations, "Paris agreement", in *Report of the Conference of the Parties to the United Nations Framework Convention on Climate Change (21st Session, 2015: Paris). Retrived December*, vol. 4, 2015, p. 2017.

[6] S. Bouckaert *et al.*, "Net zero by 2050: A roadmap for the global energy sector", 2021.

[7] National Grid, "Undergrounding high voltage electricity transmission lines", vol. 4, Jan. 2015, (Accessed on 01/18/2023).

[8] R. Huang et al, "Cable tunnel thermal rating prediction using support vector regression", in *2014 International Conference on Probabilistic Methods Applied to Power Systems (PMAPS)*, 2014, pp. 1–6. DOI: 10.1109/PMAPS.2014.6960629.

[9] H. Brakelmann and G. J. Anders, "Increasing ampacity of cables by an application of ventilated pipes", in *Conference Record of the 2004 IEEE Industry Applications Conference, 2004. 39th IAS Annual Meeting.*, vol. 4, 2004, 2288–2295 vol.4. DOI: 10.1109/IAS.2004.1348794.

[10] G. J. Anders, *Rating of Electric Power Cables in Unfavourable Thermal Environment*. IEEE Press, 2005.

[11] M. Labus and K. Labus, "Thermal conductivity and diffusivity of fine-grained sedimentary rocks", *Journal of Thermal Analysis and Calorimetry*, vol. 132, no. 3, pp. 1669–1676, 2018, ISSN: 1588-2926. DOI: 10.1007/s10973-018-7090-5. [Online]. Available: https://doi.org/10.1007/s10973-018-7090-5.

[12] R. J. Osczevski, "The basis of wind chill", *Arctic*, vol. 48, pp. 372–382, 1995.

[13] International Electrotechnical Commission, "Electric cables - Calculation of the current rating - Part 1-1: Current rating equations (100 % load factor) and calculation of losses - General", International Electrotechnical Commission, Standard, 2006. [Online]. Available: https://webstore.iec.ch/publication/1265.

[14] M Høyer-Hansen et al., "Optimisation of power cable ampacity in offshore wind farm applications", *Journal of Physics: Conference Series*, vol. 2362, no. 1, p. 012 019, Nov. 2022. DOI: 10.1088/1742-6596/2362/1/012019.

[15] S. K. Ganguli and V. Kohli, *Power cable technology*. CRC Press, 2016.

[16] C. Globe, *What is electrical power cable? definition & construction of cable - circuit globe*, https://circuitglobe.com/electrical-power-cable.html, (Accessed on 01/19/2023).

[17] R. Suchantke, "Alternating current loss measurement of power cable conductors with large cross sections using electrical methods (phd thesis)", Ph.D. dissertation, Sep. 2018. DOI: 10.14279/depositonce-7345.

[18] X.H. Wang et al., "Tackling sheath problems: Latest research developments in solving operational sheath problems in underground power transmission cables", *Electric Power Systems Research*, vol. 77, no. 10, pp. 1449–1457, 2007, ISSN: 0378-7796. DOI: https://doi.org/10.1016/j.epsr.2006.10.004.

[19] W. Jones, "More heat, less sag [power cable upgrades]", *IEEE Spectrum*, vol. 43, no. 6, pp. 16–18, 2006. DOI: 10.1109/MSPEC.2006.1638038.

[20] K. A. Rosvold, *Frekvens – nettfrekvens – store norske leksikon*, https://snl.no/frekvens_-_nettfrekvens, (Accessed on 01/25/2023), Jul. 2018.

[21] S. P. Fuchs, *Partial discharge and corona theory and measurement*, 1993. [Online]. Available: https://ecommons.udayton.edu/graduate_theses/2777.

[22] J. Su et al., "Electrical tree degradation in high-voltage cable insulation: Progress and challenges", *High Voltage*, vol. 5, no. 4, pp. 353–364, 2020. DOI: https://doi.org/10.1049/hve.2020.0009.

[23] M. Azizian Fard et al., "Electrical treeing in power cable insulation under harmonics superimposed on unfiltered hvdc voltages", *Energies*, vol. 12, no. 16, 2019, ISSN: 1996-1073. DOI: 10.3390/en12163113.

[24] G. Yilmaz and S. E. Karlik, "A distributed optical fiber sensor for temperature detection in power cables", *Sensors and Actuators A: Physical*, vol. 125, no. 2, pp. 148–155, 2006, ISSN: 0924-4247. DOI: https://doi.org/10.1016/j.sna.2005.06.024.

[25] BRUGG Kabel AG, "Technical user guide of high-voltage xlpe cable systems", BRUGG, Standard, 2017. [Online]. Available: https://bruggcables.com/fileadmin/site/documents/Hochspannungsanlagen/Technical_User_Guide_HV_XLPE_Cable_Systems_EN.pdf.

[26] Z. Yaodong *et al.*, "Analysis of current carrying capacity of power cable based on dts", *Journal of Physics: Conference Series*, vol. 1639, no. 1, p. 012 029, Oct. 2020. DOI: 10.1088/1742-6596/1639/1/012029.

[27] G. Feo et al., "Integrating fiber optic data in numerical reservoir simulation using intelligent optimization workflow", *Sensors*, vol. 20, no. 11, 2020, ISSN: 1424-8220. DOI: 10.3390/s20113075.

[28] H. Brakelmann, "Reinforcement of power cables crossing thermally unfavourable regions", *European Transactions on Electrical Power*, vol. 9, no. 3, pp. 199–202, 1999. DOI: https://doi.org/10.1002/etep.4450090309.

[29] B. Rehm et al., *CHAPTER TWO - Situational Problems in MPD*. Gulf Publishing Company, 2008, pp. 39–80, ISBN: 978-1-933762-24-1. DOI: https://doi.org/10.1016/B978-1-933762-24-1.50008-5.

[30] International Electrotechnical Commission, "Part 2-1: Thermal Resistance - Calculation of Thermal Resistance", International Electrotechnical Commission, Standard, 2015. [Online]. Available: https://webstore.iec.ch/publication/22097.

[31] Lede, "Technical documents 170 kv", Lede, Technical Documents, 2021.

[32] Y. Zhang and P.-Y. Ben Jar, "Comparison of mechanical properties between pe80 and pe100 pipe materials", *Journal of Materials Engineering and Performance*, vol. 25, pp. 4326–4332, 2016, ISSN: 4. DOI: https://doi.org/10.1007/s11665-016-2274-2.

[33] P. Association, *What is the meaning of the designations pe80 and pe100?*, https://www.pe100plus.com/PE-Pipes/Technical-guidance/model/Materials/mrs/What-is-the-meaning-of-the-designations-PE80-and-PE100-i254.html, (Accessed on 01/25/2023), May 2018.

[34] S. Dreckötter, *What is the standard dimension ratio (sdr)?*, https://pipeson.com/questions/question-what-is-standard-dimension-ratio-sdr/, (Accessed on 01/23/2023).

[35] Iljin Electric, "Technical documents 170 kv", Iljin Electric, Technical Documents, 2020.

[36] M. Heggås, *Modelling natural convection, radiation and conduction heat transfer of installed power cables specialization project*, Dec. 2018.

[37] Electrotechnik, *Current rating of cables in ventilated tunnels - elek software*, https://elek.com.au/articles/current-rating-of-cables-in-ventilated-tunnels/, (Accessed on 03/08/2023).

[38] Lascar Electronics, *Temperature and humidity data logger - el-usb-2*, https://www.lascarelectronics.com/easylog-el-usb-2, (Accessed on 01/23/2023).

[39] UBIBOT, *Ubibot gs1 temperature and humidity sensing device – ubibot online store*, https://store.ubibot.com/products/ubibot-gs1-temperature-and-humidity-sensing-device, (Accessed on 01/23/2023).

[40] UBIBOT, *Wind speed sensor – ubibot online store*, https://store.ubibot.com/products/wind-speed-sensor?_pos=1&_sid=169eaf130&_ss=r&variant=31870311727222, (Accessed on 01/23/2023).

[41] A. Savitzky and M. J. E. Golay, "Smoothing and differentiation of data by simplified least squares procedures.", *Analytical Chemistry*, vol. 36, no. 8, pp. 1627–1639, 1964. DOI: 10.1021/ac60214a047.

[42] M. Heggås, *Dynamic rating of power cables based upon transient temperature calculations*, 2019. [Online]. Available: http://hdl.handle.net/11250/2622625.

[43] J. J. Montaño Moreno et al., "Using the r-mape index as a resistant measure of forecast accuracy", *Psicothema*, vol. 25, pp. 500–506, Nov. 2013. DOI: 10.7334/psicothema2013.23.

[44] S. Kalogirou and G. Florides, "Measurements of ground temperature at various depths", *3rd International Conference on Sustainable Energy Technologies, Nottingham*, Jun. 2004.

8 Acknowledgements

The author thanks the International Electrotechnical Commission (IEC) for permission to reproduce Information from its International Standards. All such extracts are copyright of IEC, Geneva, Switzerland. All rights reserved. Further information on the IEC is available from www.iec.ch. IEC has no responsibility for the placement and context in which the extracts and contents are reproduced by the author, nor is IEC in any way responsible for the other content or accuracy therein.

A Python Code

```python
#!/usr/bin/env python3
# -*- coding: utf-8 -*-
"""
Created on Fri Jan 13 10:54:11 2023

@author: anders myklemyr
"""

import scipy.constants as const
import numpy as np
import matplotlib.pyplot as plt
import pandas as pd
from datetime import datetime

# %% Plot Configurations
size = 25
line_size = 3
legendsize = 25

# %% Constants
sigma_b = const.Stefan_Boltzmann
pi = const.pi

# Cables
N = 3           # Number of cables
n = 1           # Number of conductors in a cable
D_e = 0.1224    # Diameter of cable (m)
R = 1.95E-5    # Alternating current resistance of conductor at its maximum
# operating temperature (ohm/m)

theta_max = 90  # Maximum permissible conductor temperature

# From IEC 60287-2-1 2015
T2 = 0  # Due to no armour


# Tunnel and surroundngs
rho_soil = 1                # Soil thermal resistivity
L_t = 24                    # Depth of tunnel axis # Need to find average?
D_t = 0.6                   # Inner diameter of tunnel (m)
A_t = pi * (D_t / 2)**2     # Inner cross-sectional area of the tunnel
L = 235.6                   # length of tunnel
V = 1                       # Velocity of air [m/s]

```

```
45
46 # Constants
47 K_cv = 0.070                # Convection factor. For trefoil formation,
48 # experimentally determined constant for which values are given in Table
       2
49 F_m = 0.363                  # Coefficient of radiation for Three cables
      touching
50 K_t = 0.90                   # Effective emmisivity typically 0.9 for
      served cable
51 K_r = (1-F_m)/(1-(1-K_t)*F_m)  # Radiation shape factor
52
53
54 # Starting values
55 theta_a = -1                # Temperature at ground level
56 theta_at_inlet = -1         # Air temperature at tunnel inlet
57 theta_s_outlet = 0          # assumed starting temperature of the cable
58 # surface, at tunnel outlet [degree C]
59 theta_t_outlet = 0          # assumed starting temperature of the inner
      tunnel
60 # wall, at tunnel outlet [degree C]
61 theta_at_outlet = 0        # assumed starting air temperature at tunnel
      outlet
62
63 # Heat dissipation coefficient calculation
64 Z = 0.94
65 E = 0.79
66 g = 0.20
67 h = (Z / D_e**g) + E         # is the heat dissipation coefficient given
      in
68 # IEC 60287-2-1 for cables in still air (W/m2K5/4)
69
70 # %% Calculated constants
71
72 # thermal resistivity of insulation (K*m/W) (Table 1 in IEC60287-2-1)
73 rho_T = 3.5
74 d_c = 54.6  # diameter of conductor (mm)
75 t_1 = 21.0  # thickness of insulation between conductor and sheath (mm)
76 # Thermal resistance per core between one conductor and sheath (4.1.2.1
      in IEC60287-2-1)
77 T1 = (rho_T / (2 * pi)) * np.log(1 + (2 * t_1) / d_c)
78
79
80 t_3 = 4.5  # thickness of outer sheath/serving (mm)
81 D_a = 106.2  # external diameter of the metallic sheath (mm)
82 # Thermal resistance of external serving/outer sheath (4.1.4.1 in
      IEC60287-2-1)
83 T3 = (1 / (2*pi)) * rho_T * np.log(1 + ((2 * t_3) / D_a))
```

```
84
85 frequency = 50  # [Hz]
86 omega = 2 * pi * frequency
87 C = 2.6E-10  # Maximum capacitance per meter (F/m) from data sheet
88 U_0 = 76E3  # Voltage to earth from Table 1. Rated voltage in data sheet
89 tan_delta = 0.001  # Loss factors for the insulation from data sheet.
90 # Double check what filled and unfilled XLPE cable means?
91 # Dielectric losses per unit length per phase (W/m)
92 W_d = omega * C * U_0**2 * tan_delta
93
94
95 s = 230  # distance between conductor axes in the electrical section (mm
   )
96 # resistance of sheath per unit length (ohm/m) derived from resistivity
   of metal screen
97 R_s = (2.84E-8 * L) / 0.002
98 d = 106.2  # mean diameter of the sheath (mm)
99 # Reactance per unit length of sheath (ohm/m)
100 X = 2 * omega * 1E-7 * np.log((2 * s) / d)
101 # 2.3.1 Losses by circulating currents
102 L1_mark = (R_s / R)*(1 + (R_s / X)**2)**-1
103
104 # Calculation of power losses in the sheath
105
106 D_s = D_a  # external diameter of cable sheath (mm)
107 p_s = 2.84E-8  # electrical resisitivty of sheath material at operating
   temperature
108 t_s = 1.2  # thickness of sheath
109 m = (omega * 1E-7) / R_s
110
111 if m <= 0.1:  # three single core cables in trefoil formation
112     delta_1 = 0
113     delta_2 = 0
114 else:
115     delta_1 = (1.14 * m**(2.45) + 0.33) * (d / (2 * s))**(0.92 * m +
   1.66)
116     delta_2 = 0
117
118 # three single core cables in trefoil formation
119 lambd_0 = 3 * (m**2 / (1 + m**2)) * (d / (2 * s))**2
120
121 beta_1 = np.sqrt((4 * np.pi * omega) / (10**7 * p_s))
122 g_s = 1 + (t_s / D_s)**1.74 * (beta_1 * D_s * 10**(-3) - 1.6)
123 lambd_1_doublemark = (R_s / R) * (g_s * lambd_0 *
124                                   (1 + delta_1 + delta_2) + ((beta_1 *
   t_s)**4) / (12E12))
125 M = N_ = R_s / X  # for cables in trefoil formation
```

```
126 F = (4 * M**2 * N_**2 + (M + N_)**2) / (4 * (M**2 + 1) * (N_**2 + 1))
127 L1_doublemark = lambd_1_doublemark * F  # Losses by eddy currents
128
129
130 # 2.3 Loss factor for sheath and screen in IEC 60287-1-1
131 L1 = L1_mark + L1_doublemark
132
133
134 L2 = 0  # Lambda_2 Ratio of losses in armour to total conductor loss
135
136 # %% Calculation of thermal resistances T_st, T_as, T_at
137
138
139 def T_st_func(theta_s_outlet, theta_t_outlet):
140     """
141     4.2.3 Heat transfer by radiation from the cable surface to the inner
        wall
142     of the tunnel.
143
144     Parameters
145     ----------
146     theta_s_outlet : Temperature of the cable surface, at tunnel outlet
147     theta_t_outlet : Temperature of the inner tunnel wall, at tunnel
        outlet
148
149     Returns
150     -------
151     T_st : Radiation thermal resistance between cable and inner wall of
        the
152     tunnel  K  m/W
153
154     """
155     T_st = (pi * D_e * K_t * K_r * sigma_b * ((theta_s_outlet + 273)**2
        +
156             (theta_t_outlet + 273)**2))**-1 * ((theta_s_outlet + 273) +
        (theta_t_outlet + 273))**-1
157     return T_st
158
159
160 T_st = T_st_func(theta_s_outlet, theta_t_outlet)
161
162
163 nu = 1.32E-5 + 9.5E-8 * theta_at_outlet  # Kinematic viscosity for air [
        m2/s]
164
165 Re_air = (V * D_e) / nu  # Reynolds number
166
```

```
k_air = 2.42E-2 + 7.2E-5 * theta_at_outlet  # thermal conductivity for
# air (W/m/K)


def T_as_func(T_st, theta_s_outlet, theta_at_outlet, Re_air):
    """
    4.2.4 Heat transfer by convection from the cable surface to the air
    inside the tunnel

    Parameters
    ----------
    T_st : Radiation thermal resistance between cable and inner wall of
    the tunnel  K  m/W
    theta_s_outlet : Temperature of the cable surface, at tunnel outlet
    theta_at_outlet : Air temperature at tunnel outlet

    Returns
    -------
    T_as : Convection thermal resistance between cable and air  K  m/W

    """
    if Re_air == 0:
        T_as = 0
    elif Re_air < 2000:
        T_as = ((pi * D_e * h
                 - (1 / (30**(1/4) * T_st))) * (theta_s_outlet
                                                - theta_at_outlet)
   **(1/4))**-1
    # Laminar air flow
    else:
        T_as = (pi * k_air * K_cv * Re_air**0.65)**-1  # Turbulent air
   flow

    return T_as


T_as = T_as_func(T_st, theta_s_outlet, theta_at_outlet, Re_air)


Re_tunnel = (V * D_t) / nu

Pr = 0.715 - (2.5E-4 * theta_at_outlet)  # Prandtl number
C_pair = Pr * (k_air/nu)  # Specific heat of air per unit volume [J/m3/K
   ]

Pr = C_pair * (nu/k_air)  # Prandtl number

```

```
211
212 def T_at_func(k_air, Re_tunnel, Pr):
213     """
214     #4.2.5 Heat transfer by convection from the air inside the tunnel to
        the
215     inner tunnel wall.
216
217     Parameters
218     ----------
219     k_air : Thermal conductivity for air (W/m/K)
220     Re_tunnel : Reynolds number for the tunnel
221
222     Pr : Prandtl number
223
224     Returns
225     -------
226     T_at : Convection thermal resistance between air and inner wall of
        the
227     tunnel K m/W
228
229     """
230
231     if Re_tunnel > 2500:  # Turbulent air flow
232         T_at = (pi * k_air * 0.023 * Re_tunnel**0.8 * Pr**0.4)**-1
233     else:
234         T_at = 0  # Else thermal resistance is considered negligible
235     return T_at
236
237
238 T_at = T_at_func(k_air, Re_tunnel, Pr)
239
240 # %% Calculation of thermal resistances T_s, T_t and T_a
241
242
243 def T_s_func(T_st, T_as, T_at):
244     """
245     Equation 12: Equivalent star thermal resistance of cable [K*m/W]
246
247     Parameters
248     ----------
249     T_st : Radiation thermal resistance between cable and inner wall of
        the
250     tunnel K m/W
251     T_as : Convection thermal resistance between cable and air K m/W
252     T_at : Convection thermal resistance between air and inner wall of
        the
253         tunnel K m/W
```

```
254
255     Returns
256     -------
257     T_s : Equivalent star thermal resistance of cable [K*m/W]
258     """
259     A = (T_st/N) * (T_as/N)
260     B = (T_st/N) + (T_as/N) + (T_at)
261     T_s = A/B
262     return T_s
263
264
265 def T_t_func(T_at, T_st, T_as):
266     """
267     Equation 12: Equivalent star thermal resistance of tunnel wall [K*m/
    W]
268
269     Parameters
270     ----------
271     T_st : Radiation thermal resistance between cable and inner wall of
    the
272     tunnel K m/W
273     T_as : Convection thermal resistance between cable and air K m/W
274     T_at : Convection thermal resistance between air and inner wall of
    the
275         tunnel K m/W
276
277     Returns
278     -------
279     T_t : Equivalent star thermal resistance of tunnel wall [K*m/W]
280
281     """
282     A = (T_at) * (T_st/N)
283     B = (T_st/N) + (T_as/N) + (T_at)
284     T_t = A/B
285     return T_t
286
287
288 def T_a_func(T_at, T_as, T_st):
289     """
290     Equation 12: Equivalent star thermal resistance of air [K*m/W]
291
292     Parameters
293     ----------
294     T_st : Radiation thermal resistance between cable and inner wall of
    the
295     tunnel K m/W
296     T_as : Convection thermal resistance between cable and air K m/W
```

```
297     T_at : Convection thermal resistance between air and inner wall of
        the
298         tunnel  K  m/W
299 
300     Returns
301     -------
302     T_a : Equivalent star thermal resistance of air [K*m/W]
303 
304     """
305     A = (T_at) * (T_as/N)
306     B = (T_st/N) + (T_as/N) + (T_at)
307     T_a = A/B
308     return T_a
309 
310 
311 T_s = T_s_func(T_st, T_as, T_at)
312 T_t = T_t_func(T_at, T_st, T_as)
313 T_a = T_a_func(T_at, T_as, T_st)
314 
315 # %% Calculating permissible current rating for the cable
316 
317 C_av = C_pair * V * A_t  # specific heat of the air flow (W/K)
318 
319 mu = (2 * L_t) / D_t
320 
321 T_e = (rho_soil / (2 * pi)) * np.log(mu + np.sqrt(mu**2 - 1))  # thermal
322 # resistance of the surrounding soil
323 
324 
325 def L_0_func(T_a, T_t, C_av):
326     """
327     Reference length (m)
328 
329     Parameters
330     ----------
331     T_a : Equivalent star thermal resistance of air [K*m/W]
332     T_t : Equivalent star thermal resistance of tunnel wall [K*m/W]
333 
334     Returns
335     -------
336     L_0 : Reference length (m)
337 
338     """
339     L_0 = (T_a + T_t + T_e) * C_av
340     return L_0
341 
342 
```

```
343 L_0 = L_0_func(T_a, T_t, C_av)  # Reference length (m)
344
345
346 def T4_t_func(T_s, T_t, L_0):
347     """
348     Equivalent thermal resistance of cable surrounding (K.m/W)
349
350     Parameters
351     ----------
352     T_s : Equivalent star thermal resistance of cable [K*m/W]
353     T_t : Equivalent star thermal resistance of tunnel wall [K*m/W]
354     L_0 : Reference length (m)
355
356     Returns
357     -------
358     T4_t : Equivalent thermal resistance of cable surrounding (K.m/W)
359
360     """
361     T4_t = N * (T_s + (T_t + T_e) * (1 - ((T_t + T_e) / (T_a + T_t + T_e
    )) *
362                                       np.exp(-L/L_0)))
363
364     return T4_t
365
366
367 T4_t = T4_t_func(T_s, T_t, L_0)
368
369
370 def d_theta_0_func(T_t, T_a, L_0):
371     """
372     Fictitious increase of ambient temperature to account for the
373     ventilation (K)
374
375     Parameters
376     ----------
377     T_t : Equivalent star thermal resistance of tunnel wall [K*m/W]
378     T_a : Equivalent star thermal resistance of air [K*m/W]
379     L_0 : Reference length (m)
380
381     Returns
382     -------
383     d_theta_0 : Fictitious increase of ambient temperature to account
    for the
384     ventilation (K)
385
386     """
387     d_theta_0 = (theta_at_inlet -
```

```
                theta_a) * ((T_t + T_e) / (T_a + T_t + T_e)) * np.exp(-L/L_0)

    return d_theta_0


d_theta_0 = d_theta_0_func(T_t, T_a, L_0)


def current_rating(d_theta_0, T4_t):
    """
    Current permissible rating

    Parameters
    ----------
    d_theta_0 : Fictitious increase of ambient temperature to account for the
    ventilation (K)
    T4_t : Equivalent thermal resistance of cable surrounding (K.m/W)

    Returns
    -------
    I : Current permissible rating (A)
    """
    A = theta_max - (theta_a + d_theta_0) - W_d * ((T1 / 2) + n * (T2 + T3
                                                                   +
    T4_t))
    B = R * (T1 + n * (1 + L1) * T2 + n * (1 + L1 + L2) * (T3 + T4_t))
    I = (A / B)**(1 / 2)
    return I


I = current_rating(d_theta_0, T4_t)

# %% Losses in the cable

W_c = R * I**2  # losses in a conductor per unit length, assuming maximum
# conductor temperature (W/m)


W_k = n * (W_c * (1 + L1 + L2) + W_d)  # Total heat generated by cable (W/m)

# %% Air temp at tunnel outlet, cable surface temp and tunnel wall temp
# calculations
```

```
429
430
431 def theta_at_outlet_func(T_t, W_k, L_0):
432     """
433     The air temperature at tunnel outlet
434
435     Parameters
436     ----------
437     T_t : Equivalent star thermal resistance of tunnel wall [K*m/W]
438     W_k : Total heat generated by cable (W/m)
439     L_0 : Reference length (m)
440
441     Returns
442     -------
443     theta_at_outlet : The air temperature at tunnel outlet
444
445     """
446     theta_at_outlet = theta_at_inlet + (theta_a + (T_t + T_e) * N * W_k
    -
447                                         theta_at_inlet) * (1 - np.exp(-L
    /L_0))
448     return theta_at_outlet
449
450
451 theta_at_outlet = theta_at_outlet_func(T_t, W_k, L_0)
452
453 W_a_outlet = ((T_t + T_e) * N * W_k -
454               (theta_at_outlet - theta_a)) / (T_a + T_t + T_e)
455 # heat removed by the air at tunnel outlet
456
457
458 def theta_s_outlet_func(T_a, W_a_outlet, T_s, W_k):
459     """
460     cable surface temperature
461
462     Parameters
463     ----------
464     T_a : Equivalent star thermal resistance of air [K*m/W]
465     W_a_outlet : heat removed by the air at tunnel outlet
466     T_s : TYPE
467         DESCRIPTION.
468     W_k : Total heat generated by cable (W/m)
469
470     Returns
471     -------
472     theta_s_outlet :  cable surface temperature
473
```

```
474     """
475     theta_s_outlet = theta_at_outlet + T_a * W_a_outlet + T_s * N * W_k
476 
477     return theta_s_outlet
478 
479 
480 def theta_t_outlet_func(T_a, W_a_outlet, T_t, W_k):
481     """
482     The tunnel wall temperature at tunnel outlet
483 
484     Parameters
485     ----------
486     T_a : Equivalent star thermal resistance of air [K*m/W]
487     W_a_outlet : Heat removed by the air at tunnel outlet
488     T_t : Equivalent star thermal resistance of tunnel wall [K*m/W]
489     W_k : Total heat generated by cable (W/m)
490 
491     Returns
492     -------
493     theta_t_outlet : The tunnel wall temperature at tunnel outlet
494 
495     """
496     theta_t_outlet = theta_at_outlet + T_a * W_a_outlet - T_t * (N * W_k
497                                                                  -
    W_a_outlet)
498 
499     return theta_t_outlet
500 
501 
502 theta_s_outlet = theta_s_outlet_func(T_a, W_a_outlet, T_s, W_k)
503 theta_t_outlet = theta_t_outlet_func(T_a, W_a_outlet, T_t, W_k)
504 
505 # %% Iterative process
506 
507 epsilon = 1e-5
508 theta_s_outlet_list = []
509 theta_t_outlet_list = []
510 theta_at_outlet_list = []
511 
512 theta_s_outlet_list.extend([0, 1])
513 theta_t_outlet_list.extend([0, 1])
514 theta_at_outlet_list.extend([0, 1])
515 
516 
517 # Main calculation function
518 def calc_ampacity(V):
519     """
```

```
520     Main iterative process calculation of current carrying capacity
521     Calculation is repeated until cable surface temp, tunnel wall temp,
    and air
522     temp converges and are stable.
523 
524     Parameters
525     ----------
526     V : Air velocity (m/s)
527 
528     Returns
529     -------
530     I : Current carrying capacity
531     theta_at_outlet_list : List of air temperatures at the tunnel outlet
        as the
532     program is converging
533 
534     """
535     d_theta_s_outlet = 1
536     d_theta_t_outlet = 1
537     d_theta_at_outlet = 1
538 
539     if abs(d_theta_at_outlet) > epsilon and abs(d_theta_s_outlet) >
    epsilon and abs(d_theta_t_outlet) > epsilon:
540         while abs(d_theta_at_outlet) > epsilon and abs(d_theta_s_outlet)
        > epsilon and abs(d_theta_t_outlet) > epsilon:
541 
542             T_st = T_st_func(theta_s_outlet_list[-1],
    theta_t_outlet_list[-1])
543 
544             # Kinematic viscosity
545             nu = 1.32E-5 + 9.5E-8 * theta_at_outlet_list[-1]
546             # for air [m2/s]
547             Re_air = (V * D_e) / nu  # Reynolds number
548             k_air = 2.42E-2 + 7.2E-5 * theta_at_outlet_list[-1]  #
    thermal
549             # conductivity for air (W/m/K)
550 
551             T_as = T_as_func(T_st, theta_s_outlet_list[-1],
552                              theta_at_outlet_list[-1], Re_air)
553 
554             Re_tunnel = (V * D_t) / nu
555 
556             Pr = 0.715 - (2.5E-4 * theta_at_outlet_list[-1])  # Prandtl
    number
557             # Specific heat of air per unit volume [J/m3/K]
558             C_pair = Pr * (k_air / nu)
559 
```

```
560             Pr = C_pair * (nu / k_air)  # Prandtl number
561
562             T_at = T_at_func(k_air, Re_tunnel, Pr)
563
564             T_s = T_s_func(T_st, T_as, T_at)
565             T_t = T_t_func(T_at, T_st, T_as)
566             T_a = T_a_func(T_at, T_as, T_st)
567
568             C_av = C_pair * V * A_t
569
570             L_0 = L_0_func(T_a, T_t, C_av)
571             T4_t = T4_t_func(T_s, T_t, L_0)
572             d_theta_0 = d_theta_0_func(T_t, T_a, L_0)
573             I = current_rating(d_theta_0, T4_t)
574
575             # Losses
576             W_c = R * (I**2)
577             W_k = n * (W_c * (1 + L1 + L2) + W_d)
578
579             theta_at_outlet = theta_at_outlet_func(T_t, W_k, L_0)
580             W_a_outlet = ((T_t + T_e) * N * W_k - (theta_at_outlet
581                                                    - theta_a)) / (T_a +
    T_t + T_e)
582
583             theta_s_outlet = theta_s_outlet_func(T_a, W_a_outlet, T_s,
    W_k)
584             theta_t_outlet = theta_t_outlet_func(T_a, W_a_outlet, T_t,
    W_k)
585
586             theta_s_outlet_list.append(theta_s_outlet)
587             theta_t_outlet_list.append(theta_t_outlet)
588             theta_at_outlet_list.append(theta_at_outlet)
589
590             d_theta_s_outlet = theta_s_outlet_list[-1] - \
591                 theta_s_outlet_list[-2]
592             d_theta_t_outlet = theta_t_outlet_list[-1] - \
593                 theta_t_outlet_list[-2]
594             d_theta_at_outlet = theta_at_outlet_list[-1] - \
595                 theta_at_outlet_list[-2]
596
597         return I, theta_at_outlet, theta_at_outlet_list
598
599     else:
600         raise
601
602
603 V_list = np.arange(0, 20.5, 0.5)
```

```
current = []
tunnel_outlet = []
for V in V_list:
    I, theta_at_outlet, theta_at_outlet_list = calc_ampacity(V)
    current.append(I)
    tunnel_outlet.append(theta_at_outlet)


# %% Plot with varying outside temperature

theta_s_outlet_list = []
theta_t_outlet_list = []
theta_at_outlet_list = []

theta_s_outlet_list.extend([0, 1])
theta_t_outlet_list.extend([0, 1])
theta_at_outlet_list.extend([0, 1])

T_outside_list = np.arange(-30, 40, 10)

for t in T_outside_list:
    theta_a = t
    current = []
    tunnel_outlet = []
    V_list = np.arange(0, 20.5, 0.5)
    for V in V_list:
        I, theta_at_outlet, theta_at_outlet_list = calc_ampacity(V)
        current.append(I)
        tunnel_outlet.append(theta_at_outlet)
    plt.plot(V_list, current, label=str(t) +
             r' $\degree C$', linewidth=line_size)


plt.xlim(0, 11)
plt.ylim(900, 2550)
plt.xticks(fontsize=size)
plt.yticks(fontsize=size)
plt.title("Current carrying capacity with respect to velocity of air",
    fontsize=size)
plt.legend(loc='lower right', fontsize=legendsize)
plt.grid()
plt.ylabel("Current [A]", fontsize=size)
plt.xlabel("Natural velocity of air [m/s]", fontsize=size)
plt.rcParams["figure.autolayout"] = True


# %% #%% Estimation of induced wind in a circular tunnel
```

```
650
651 g = 9.81
652 height = 78.803-27.756
653 T_i = -5
654 T_o = 5
655 average_air_temp = (T_i + T_o) / 2
656
657 D_equivalent = np.sqrt((((D_t/2)**2 * pi) - ((D_e*4)/2)**2 * pi) / (pi))
658
659
660 def induced_wind(T_i, T_o, Re_wind):
661
662     delta_p = 3417.12*height * (1/(T_i+273) - 1/(T_o+273))
663
664     l_p = L + 2 * height
665     rho = 352.64 / (average_air_temp + 273)
666
667     friction = (1.82*np.log10(Re_wind)-1.64)**-2
668
669     w = np.sqrt((2 * delta_p * D_equivalent)/(l_p * rho * friction))
670
671     return w
672
673
674 T_i_list = np.arange(-30, 35, 5)
675
676
677 for i, inlet_temp in enumerate(T_i_list[0:-2]):
678     T_o_list = np.arange(inlet_temp + 1, 30)
679     w_list = []
680     w = 1E-5
681     for T in T_o_list:
682
683         nu_w = 1.32E-5 + 9.5E-8 * T  # Kinematic viscosity for air [m2/s
    ]
684         Re_wind = (w * D_e) / nu_w  # Reynolds number
685
686         w = induced_wind(inlet_temp, T, Re_wind)
687         w_list.append(w)
688
689     plt.plot(T_o_list, w_list, label=str(inlet_temp) +
690              r' $\degree C$', linewidth=line_size)
691
692
693 plt.title(
694     "Naturally induced wind in cable tunnel with varying outlet temp",
    fontsize=size)
```

```
695 plt.ylim(0, 2.1)
696 plt.xticks(fontsize=size)
697 plt.yticks(fontsize=size)
698 plt.legend(loc='upper left', fontsize=19)
699 plt.grid()
700 plt.ylabel("Induced air velocity [m/s]", fontsize=size)
701 plt.xlabel(r"Outlet air temperature [$\degree C$]", fontsize=size)
702 plt.rcParams["figure.autolayout"] = True
703 plt.text(-4.5, 1.37, '-30$\degree C$', fontsize=20,
704          bbox=dict(facecolor='grey', boxstyle="square"))
705 plt.text(0.5, 1.17, '-20$\degree C$', fontsize=20,
706          bbox=dict(facecolor='grey', boxstyle="square"))
707 plt.text(6, 0.98, '-10$\degree C$', fontsize=20,
708          bbox=dict(facecolor='grey', boxstyle="square"))
709 plt.text(12, 0.8, '0$\degree C$', fontsize=20,
710          bbox=dict(facecolor='grey', boxstyle="square"))
711 plt.text(18, 0.6, '10$\degree C$', fontsize=20,
712          bbox=dict(facecolor='grey', boxstyle="square"))
713 plt.text(24, 0.4, '20$\degree C$', fontsize=20,
714          bbox=dict(facecolor='grey', boxstyle="square"))
715
716 # %% Calculation of temperature with constant current
717
718 theta_a = 0                 # Temperature at ground level
719 theta_at_inlet = 0          # Air temperature at tunnel inlet
720 theta_s_outlet = 0           # assumed starting temperature of the cable
721 # surface, at tunnel outlet [degree C]
722 theta_t_outlet = 0          # assumed starting temperature of the inner
       tunnel
723 # wall, at tunnel outlet [degree C]
724 theta_at_outlet = 6.9        # assumed starting air temperature at tunnel
       outlet
725
726 theta_s_outlet_list = []
727 theta_t_outlet_list = []
728 theta_at_outlet_list = []
729
730 theta_s_outlet_list.extend([0, 1])
731 theta_t_outlet_list.extend([0, 1])
732 theta_at_outlet_list.extend([0, 1])
733
734 # Main calculation function
735
736
737 def calc_temp(V, I):
738     """
739     Main iterative process calculation of current carrying capacity
```

```
740     Calculation is repeated until cable surface temp, tunnel wall temp,
    and air
741     temp converges and are stable.
742 
743     Parameters
744     ----------
745     V : Air velocity (m/s)
746 
747     Returns
748     -------
749     I : Current carrying capacity
750     theta_at_outlet_list : List of air temperatures at the tunnel outlet
        as the
751     program is converging
752 
753     """
754     d_theta_s_outlet = 1
755     d_theta_t_outlet = 1
756     d_theta_at_outlet = 1
757 
758     if abs(d_theta_at_outlet) > epsilon and abs(d_theta_s_outlet) >
    epsilon and abs(d_theta_t_outlet) > epsilon:
759         while abs(d_theta_at_outlet) > epsilon and abs(d_theta_s_outlet)
        > epsilon and abs(d_theta_t_outlet) > epsilon:
760 
761             T_st = T_st_func(theta_s_outlet_list[-1],
    theta_t_outlet_list[-1])
762 
763             # Kinematic viscosity
764             nu = 1.32E-5 + 9.5E-8 * theta_at_outlet_list[-1]
765             # for air [m2/s]
766             Re_air = (V * D_e) / nu  # Reynolds number
767             k_air = 2.42E-2 + 7.2E-5 * theta_at_outlet_list[-1]  #
    thermal
768             # conductivity for air (W/m/K)
769 
770             T_as = T_as_func(T_st, theta_s_outlet_list[-1],
771                              theta_at_outlet_list[-1], Re_air)
772 
773             Re_tunnel = (V * D_t) / nu
774 
775             Pr = 0.715 - (2.5E-4*theta_at_outlet_list[-1])  # Prandtl
    number
776             # Specific heat of air per unit volume [J/m3/K]
777             C_pair = Pr * (k_air / nu)
778 
779             Pr = C_pair * (nu / k_air)  # Prandtl number
```

```
780
781             T_at = T_at_func(k_air, Re_tunnel, Pr)
782
783             T_s = T_s_func(T_st, T_as, T_at)
784             T_t = T_t_func(T_at, T_st, T_as)
785             T_a = T_a_func(T_at, T_as, T_st)
786
787             C_av = C_pair * V * A_t
788
789             L_0 = L_0_func(T_a, T_t, C_av)
790             T4_t = T4_t_func(T_s, T_t, L_0)
791             d_theta_0 = d_theta_0_func(T_t, T_a, L_0)
792             # I = 300
793
794             # Losses
795             W_c = R * (I**2)
796             W_k = n * (W_c * (1 + L1 + L2) + W_d)
797
798             theta_at_outlet = theta_at_outlet_func(T_t, W_k, L_0)
799             W_a_outlet = ((T_t + T_e) * N * W_k - (theta_at_outlet
800                                                    - theta_a)) / (T_a +
    T_t + T_e)
801
802             theta_s_outlet = theta_s_outlet_func(T_a, W_a_outlet, T_s,
    W_k)
803             theta_t_outlet = theta_t_outlet_func(T_a, W_a_outlet, T_t,
    W_k)
804
805             theta_s_outlet_list.append(theta_s_outlet)
806             theta_t_outlet_list.append(theta_t_outlet)
807             theta_at_outlet_list.append(theta_at_outlet)
808
809             d_theta_s_outlet = theta_s_outlet_list[-1] - \
810                 theta_s_outlet_list[-2]
811             d_theta_t_outlet = theta_t_outlet_list[-1] - \
812                 theta_t_outlet_list[-2]
813             d_theta_at_outlet = theta_at_outlet_list[-1] - \
814                 theta_at_outlet_list[-2]
815
816         return theta_at_outlet, theta_s_outlet
817
818     else:
819         return
820
821
822 V_list = np.arange(0, 20.5, 0.5)
823 cable_surface_outlet = []
```

```
tunnel_outlet = []
for V in V_list:
    theta_at_outlet, cable_outlet_temp = calc_temp(V, I=300)

    cable_surface_outlet.append(cable_outlet_temp)
    tunnel_outlet.append(theta_at_outlet)


plt.plot(V_list, cable_surface_outlet, linewidth=line_size)
plt.plot(V_list, tunnel_outlet, linewidth=line_size)
plt.xlim(0, 11)
plt.xticks(fontsize=size)
plt.yticks(fontsize=size)
plt.grid()
plt.title("Temperatures at outlet with varying air velocity", fontsize=
    size)
# plt.legend([r"${\theta}_s$", r"${\theta}_{at}$"], fontsize=legendsize)
plt.ylabel("Temperature [$\degree$C]", fontsize=size)
plt.xlabel("Natural velocity of air [m/s]", fontsize=size)
plt.rcParams["figure.autolayout"] = True
```

```
#!/usr/bin/env python3
# -*- coding: utf-8 -*-
"""
Created on Mon Feb  6 13:47:45 2023

@author: anders
"""

import matplotlib.pyplot as plt
import numpy as np


V = np.arange(1e-5, 11, 0.1)
h_c = 12.12 - 1.16*V + 11.6*np.sqrt(V)

size = 25

plt.plot(V, h_c, linewidth=3)
plt.ylim(8, 40)
plt.xlim(0, 11)
plt.xticks(fontsize=size)
plt.yticks(fontsize=size)
plt.grid()
plt.title('Convective heat transfer coefficient of air', fontsize=size)
plt.ylabel(r'Heat Transfer Coefficient ($W/m^2K$)', fontsize=size)
plt.xlabel('Air Velocity $(m/s)$', fontsize=size)
plt.rcParams["figure.autolayout"] = True
```

```
#!/usr/bin/env python3
# -*- coding: utf-8 -*-
"""
Created on Mon Feb 20 09:15:04 2023

@author: anders
"""

# importing packages
import numpy as np
import pandas as pd
from datetime import datetime
import matplotlib.pyplot as plt
from IEC_Calculations_170kV_cable import *
from scipy.signal import savgol_filter

# %%

bottom_data = pd.read_csv(
    '/Users/anders/Library/CloudStorage/OneDrive-NorwegianUniversityofLifeSciences/Master/Data/Data_for_Python/Bottom_Temp_dec_feb.csv')
top_data = pd.read_csv(
    '/Users/anders/Library/CloudStorage/OneDrive-NorwegianUniversityofLifeSciences/Master/Data/Data_for_Python/Top_basin_data.csv')

# cleaning up dataframe
bottom_data = bottom_data.drop(
    columns=['Comments', 'Serial Number', 'Dew Point(C)', 'Bottom Temp', 'Humidity(%rh)'])

top_data = top_data.drop(columns=['field3(Voltage)', 'field4(WIFI RSSI)', 'field5(GSM RSSI)', 'field8(RS485 Humidity)',
                          'field9(RS485 Soil Temperature)', 'field10(RS485 Soil Moisture)', 'status', 'lat', 'long', 'elev', 'wifi', 'cell', 'serial', 'field6(Light)'])

top_data.rename(columns={'field1(Temperature  C  )': 'Temperature',
                'field2(Humidity)': 'Humidity', 'field7(Wind Speed-W1)': 'Wind Speed'}, inplace=True)

# Removing the +01:00 ending of data at the top basin
top_data['created_at'] = top_data['created_at'].map(lambda x: str(x)[:-6])

# %% Converting to correct date format
```

```
38
39 bottom_data['Time'] = pd.to_datetime(bottom_data['Time'], format='%Y-%m
       -%d')
40 bottom_data = bottom_data.set_index('Time')
41
42 top_data['created_at'] = pd.to_datetime(
43     top_data['created_at'], format='%Y-%m-%d')
44
45 # %% grouping entries
46
47 top_data = top_data.groupby(pd.Grouper(key='created_at', freq='10min')).
       max()
48
49 top_data = top_data.loc['2022-12-15 13:00:00':'2023-02-17 09:00:00']
50
51 # %% Plotting overview plot
52
53 fig, ax1 = plt.subplots()
54
55 ax2 = ax1.twinx()
56 ax1.plot(bottom_data.index, bottom_data['Celsius(C)'], 'r-')
57 ax1.plot(top_data.index, top_data['Temperature'], 'b-')
58 ax2.plot(top_data.index, top_data['Wind Speed'], 'g')
59
60 ax1.set_xlabel('Date')
61 ax1.set_ylabel('Temperature [$\degree$C]')
62 ax2.set_ylabel('Wind Speed [V]')
63
64 ax1.legend(['Bottom temperature', 'Top basin temperature'])
65 ax2.legend(['Top basin wind speed'])
66
67
68 # %% Plotting time framed plot
69
70 top_data_dec = top_data.loc['2022-12-15 13:00:00':'2022-12-25 23:50:00']
71 bottom_data_dec = bottom_data.loc['2022-12-15 13:00:00':'2022-12-25
       23:50:00']
72
73 top_data_dec_wind = top_data_dec['Wind Speed'].where(
74     top_data_dec['Wind Speed'] > 0).to_frame().dropna()
75
76
77 fig, ax1 = plt.subplots()
78
79 ax2 = ax1.twinx()
80 ax1.plot(bottom_data_dec.index, bottom_data_dec['Celsius(C)'], 'r-')
81 ax1.plot(top_data_dec.index, top_data_dec['Temperature'], 'b-')
```

```
ax2.plot(top_data_dec_wind.index, top_data_dec_wind['Wind Speed'], 'go')


ax1.set_xlabel('Date')
ax1.set_ylabel('Temperature [$\degree$C]')
ax2.set_ylabel('Wind Speed [V]')
ax2.set_ylim(0, 0.8)

ax1.legend(['Bottom temperature', 'Top basin temperature'])
ax2.legend(['Top basin wind speed'])


# %% Plotting wind speed vs delta temperature between inlet and outlet

delta_T = abs(top_data_dec['Temperature'].subtract(
    bottom_data_dec['Celsius(C)']))
savgol_amp_dec = savgol_filter(
    amp_data['5m_snitt_L2'].loc['2022-12-15 00:00:00':'2022-12-25
    23:50:00'], 600, 3)  # smoothing function

savgol_delta_T = savgol_filter(
    delta_T.loc['2022-12-15 13:00:00':'2022-12-25 23:50:00'], 50, 3)  #
    filtering delta_T

fig, ax1 = plt.subplots()

ax2 = ax1.twinx()
ax3 = ax1.twinx()
ax1.plot(bottom_data_dec.index, savgol_delta_T, 'r-', linewidth=3)
ax2.plot(top_data_dec_wind.index,
         top_data_dec_wind['Wind Speed'], 'go', linewidth=1)
ax3.plot(bottom_data_dec.index, savgol_amp_dec,
         'steelblue', linewidth=line_size)


ax3.spines.right.set_position(("axes", 1.15))
ax3.spines['right'].set_color('steelblue')

ax1.set_ylabel('Temperature [$\degree$C]', fontsize=size)
ax2.set_ylabel('Wind Speed [V]', fontsize=size)
ax3.set_ylabel('Cable Load [I]', fontsize=size)

ax2.set_ylim(0, 0.8)

plt.title('Inlet and outlet temperature difference and wind speed',
    fontsize=size)

```

```
ax1.tick_params(axis='y', labelsize=size)
ax1.tick_params(axis='x', labelsize=20, labelrotation=30)
ax2.tick_params(axis='y', labelsize=size)
ax3.tick_params(axis='y', labelsize=size, colors='steelblue')
plt.rcParams["figure.autolayout"] = True


# %% Modelling based on data

amp_data = pd.read_csv(
    '/Users/anders/Library/CloudStorage/OneDrive-NorwegianUniversityofLifeSciences/Master/Data/Data_for_Python/Amperage_5min_average.csv')
amp_data['timeStamp'] = amp_data['timeStamp'].map(lambda x: str(x)[:-2])
amp_data['timeStamp'] = pd.to_datetime(
    amp_data['timeStamp'], format='%Y-%m-%d')
amp_data = amp_data.groupby(pd.Grouper(key='timeStamp', freq='10min')).mean()
amp_data = amp_data.loc['2022-12-15 13:00:00':'2023-02-17 09:00:00']
amp_data = amp_data.fillna(method='ffill')


luft_temp = pd.read_csv('/Users/anders/Library/CloudStorage/OneDrive-NorwegianUniversityofLifeSciences/Master/Data/Data_for_Python/luft_temp.csv',
                        header=0, delimiter=';', usecols=[2, 3], decimal=',')
luft_temp['Tid(norsk normaltid)'] = pd.to_datetime(
    luft_temp['Tid(norsk normaltid)'], format='%d.%m.%Y %H:%M')
luft_temp = luft_temp.groupby(pd.Grouper(
    key='Tid(norsk normaltid)', freq='10min')).mean()
luft_temp = luft_temp.fillna(method='ffill')
luft_temp = luft_temp.loc['2022-12-15 13:00:00':'2023-02-17 09:00:00']


theta_a = 0                 # Temperature at ground level
theta_at_inlet = 0          # Air temperature at tunnel inlet
theta_s_outlet = 0           # assumed starting temperature of the cable
# surface, at tunnel outlet [degree C]
theta_t_outlet = 0          # assumed starting temperature of the inner tunnel
# wall, at tunnel outlet [degree C]
theta_at_outlet = 0        # assumed starting air temperature at tunnel outlet

theta_s_outlet_list = []
theta_t_outlet_list = []
```

```
theta_at_outlet_list = []

theta_s_outlet_list.extend([0, 1])
theta_t_outlet_list.extend([0, 1])
theta_at_outlet_list.extend([0, 1])

cable_surface_outlet = []
air_outlet = []
ambient_temp = []
V = 0

for amp, bottom_temp, luft_temp_ in zip(amp_data['5m_snitt_L2'],
    bottom_data['Celsius(C)'], luft_temp['Lufttemperatur']):
    theta_a = luft_temp_
    theta_at_inlet = bottom_temp
    air_outlet_temp, cable_surface_temp = calc_temp(V, amp)
    air_outlet.append(air_outlet_temp)
    # cable_surface_outlet.append(cable_surface_temp)
    ambient_temp.append(luft_temp_)

amp_data['air_temp_outlet'] = air_outlet  # calculated
amp_data['air_temp_inlet'] = bottom_data['Celsius(C)']  # from data
amp_data['ambient_temp'] = luft_temp['Lufttemperatur']  # from data


# %% Plotting model and data together
fig, ax1 = plt.subplots()


savgol_amp = savgol_filter(
    amp_data['5m_snitt_L2'], 600, 3)  # smoothing function
savgol_outlet_temp = savgol_filter(
    amp_data['air_temp_outlet'], 600, 3)  # smoothing function


ax1.plot(top_data.index, savgol_filter(
    top_data['Temperature'], 600, 3), 'b-')  # outlet temp data


# model based outlet temperature
ax1.plot(amp_data.index, savgol_outlet_temp, 'Orange')

ax1.set_ylabel('Temperature [$\degree$C]', fontsize=size)

plt.title('Modelled- and data-based outlet temperature ', fontsize=size)

ax1.set_ylim(0, 10)
```

```
ax1.tick_params(axis='y', labelsize=size)
ax1.tick_params(axis='x', labelsize=20, labelrotation=30)
ax2.tick_params(axis='y', labelsize=size)
plt.rcParams["figure.autolayout"] = True


# Calculating MAPE for the model

# Defining MAPE function
def MAPE(Y_actual, Y_Predicted):
    mape = np.mean(np.abs((Y_actual - Y_Predicted)/Y_actual))*100
    return mape


Y_Predicted = savgol_filter(amp_data['air_temp_outlet'], 600, 3)
Y_actual = savgol_filter(top_data['Temperature'], 600, 3)
mape = MAPE(Y_actual, Y_Predicted)


# %% Filtering the data and plotting
size = 25
line_size = 2
legendsize = 20

fig, ax1 = plt.subplots()

ax2 = ax1.twinx()

# raw data
ax1.plot(bottom_data.index, bottom_data['Celsius(C)'],
         'lightcoral', alpha=0.5, linewidth=line_size)  # data
ax1.plot(top_data.index, top_data['Temperature'],
         'lightskyblue', alpha=0.5, linewidth=line_size)  # data
ax2.plot(amp_data.index, amp_data['5m_snitt_L2'], 'lightgreen',
         alpha=0.5, linewidth=line_size)  # data from cable

# filtered data

savgol_amp = savgol_filter(
    amp_data['5m_snitt_L2'], 600, 3)  # smoothing function
savgol_outlet_temp = savgol_filter(
    top_data['Temperature'], 600, 3)  # smoothing function
savgol_bottom_temp = savgol_filter(bottom_data['Celsius(C)'], 600, 3)


# Plotting raw data with filtered data
ax1.plot(amp_data.index, savgol_bottom_temp, 'red', linewidth=line_size)
```

```
ax1.plot(amp_data.index, savgol_outlet_temp, 'blue', linewidth=line_size)
ax2.plot(amp_data.index, savgol_amp, 'green', linewidth=line_size)

plt.title('Temperature and amperage data before and after filtering', fontsize=size)

ax1.set_ylabel('Temperature [$\degree$C]', fontsize=size)
ax2.set_ylabel('Cable load [I]', fontsize=size)


ax1.tick_params(axis='y', labelsize=size)
ax1.tick_params(axis='x', labelsize=20, labelrotation=30)
ax2.tick_params(axis='y', labelsize=size)
plt.rcParams["figure.autolayout"] = True


# %% Filtered Data with wind speed

delta_T_all = abs(top_data['Temperature'].subtract(bottom_data['Celsius(C)']))
savgol_delta_T_all = savgol_filter(delta_T_all, 600, 3)  # filtering delta_T

fig, ax1 = plt.subplots()
ax2 = ax1.twinx()
ax3 = ax1.twinx()
ax3.spines.right.set_position(("axes", 1.15))
ax3.spines['right'].set_color('red')

ax1.plot(amp_data.index, savgol_delta_T_all, 'blue', linewidth=line_size)
ax2.plot(top_data_dec_wind.index,
         top_data_dec_wind['Wind Speed'], 'o', color='magenta')
ax3.plot(amp_data.index, savgol_amp, 'limegreen', linewidth=line_size)


plt.rcParams["figure.autolayout"] = True


# %% DTS- FIBER Data

dts_pd_22 = pd.read_csv(
    '/Users/anders/Library/CloudStorage/OneDrive-NorwegianUniversityofLifeSciences/Master/Data/Kabeldata/Export_2022-12-14-23-00-26_DTS_Circuit 1.txt', sep='\s+', header=7, decimal=',')
dts_pd_22 = dts_pd_22.drop(
```

```
    columns=['5', 'Zone.5', '6', 'Zone.6', '7', 'Zone.7', '8'])
dts_pd_22.columns = ['Time', 'Zone 1', 'Zone 2', 'Zone 3',
                     'Zone 4', 'Zone 5', 'Zone 6', 'Zone 7', 'Zone 8']
dts_pd_22 = dts_pd_22.drop(
    columns=['Zone 1', 'Zone 2', 'Zone 3', 'Zone 4', 'Zone 5', 'Zone 6',
    'Zone 8'])

dts_pd_22['Time'] = dts_pd_22['Time'].map(lambda x: str(x)[:-4])
dts_pd_22['Time'] = pd.to_datetime(dts_pd_22['Time'], format='%Y-%m-%d %
   H:%M')
dts_pd_22 = dts_pd_22.groupby(pd.Grouper(key='Time', freq='10min')).mean
   ()
dts_pd_22 = dts_pd_22.loc['2022-12-15 13:00:00':'2023-02-17 09:00:00']


dts_pd_23 = pd.read_csv(
    '/Users/anders/Library/CloudStorage/OneDrive-
   NorwegianUniversityofLifeSciences/Master/Data/Kabeldata/Export_2023
   -01-01-00-02-31_DTS_Circuit 1.txt', sep='\s+', header=7, decimal=',')
dts_pd_23 = dts_pd_23.drop(
    columns=['5', 'Zone.5', '6', 'Zone.6', '7', 'Zone.7', '8'])

dts_pd_23.columns = ['Time', 'Zone 1', 'Zone 2', 'Zone 3',
                     'Zone 4', 'Zone 5', 'Zone 6', 'Zone 7', 'Zone 8']

dts_pd_23 = dts_pd_23.drop(
    columns=['Zone 1', 'Zone 2', 'Zone 3', 'Zone 4', 'Zone 5', 'Zone 6',
    'Zone 8'])

dts_pd_23['Time'] = dts_pd_23['Time'].map(lambda x: str(x)[:-4])
dts_pd_23['Time'] = pd.to_datetime(dts_pd_23['Time'], format='%Y-%m-%d %
   H:%M')
dts_pd_23 = dts_pd_23.groupby(pd.Grouper(key='Time', freq='10min')).mean
   ()
dts_pd_23 = dts_pd_23.loc['2022-12-15 13:00:00':'2023-02-17 09:00:00']

dts_pd = dts_pd_22.append(dts_pd_23)

savgol_dts = savgol_filter(dts_pd['Zone 7'], 600, 3)  # smoothing
   function


plt.plot(dts_pd.index, savgol_dts, 'darkviolet',
         linewidth=line_size, label='Cable temperature')
plt.plot(dts_pd.index, savgol_bottom_temp, 'red',
         linewidth=line_size, label='Inlet temperature')
plt.title('Cable- and inlet temperatures', fontsize=size)
```

```
336
337 plt.ylabel('Temperature [$\degree$C]', fontsize=size)
338 # plt.legend()
339
340 plt.tick_params(axis='y', labelsize=size)
341 plt.tick_params(axis='x', labelsize=20, labelrotation=30)
342
343 plt.rcParams["figure.autolayout"] = True
```

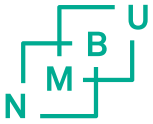

Norges miljø- og biovitenskapelige universitet
Noregs miljø- og biovitskapelege universitet
Norwegian University of Life Sciences

Postboks 5003
NO-1432 Ås
Norway